nature microbiology

Article

https://doi.org/10.1038/s41564-024-01910-8

Streptomyces secretes a siderophore that sensitizes competitor bacteria to phage infection

Received: 5 February 2024

Accepted: 6 December 2024

Published online: 08 January 2025

Check for updates

Zhiyu Zang[1], Chengqian Zhang[1], Kyoung Jin Park[1], Daniel A. Schwartz[2], Ram Podicheti[3], Jay T. Lennon[2] & Joseph P. Gerdt[1]

To overtake competitors, microbes produce and secrete secondary metabolites that kill neighbouring cells and sequester nutrients. This metabolite-mediated competition probably evolved in complex microbial communities in the presence of viral pathogens. We therefore hypothesized that microbes secrete natural products that make competitors sensitive to phage infection. We used a binary-interaction screen and chemical characterization to identify a secondary metabolite (coelichelin) produced by *Streptomyces* sp. that sensitizes its soil competitor *Bacillus subtilis* to phage infection in vitro. The siderophore coelichelin sensitized *B. subtilis* to a panel of lytic phages (SPO1, SP10, SP50, Goe2) via iron sequestration, which prevented the activation of *B. subtilis* Spo0A, the master regulator of the stationary phase and sporulation. Metabolomics analysis revealed that other bacterial natural products may also provide phage-mediated competitive advantages to their producers. Overall, this work reveals that synergy between natural products and phages can shape the outcomes of competition between microbes.

Competition is a common theme in microbial life[1]. Given the finite resources and space in their niches, microbes have evolved an arsenal of strategies that allow them to persist in the face of competition with other microorganisms[2]. The secretion of secondary metabolites is one of the most common methods by which bacteria and fungi compete with neighbouring microbes[1,2]. For example, secreted metabolites frequently kill competitors[3], prevent their attachment to surfaces[4] and starve them of essential nutrients[5].

To find new mechanisms of natural product-based microbial competition, we considered environmental factors that microbes might leverage for competitive advantage. Since microbes naturally compete within populations that interact with other predators and pathogens, we investigated whether microbes secrete metabolites that sensitize their competitors to the ubiquitous predators or pathogens around them. The major pathogens of bacteria are bacteriophage viruses (phages)[6]. These obligate parasites are strong agents of selection that can induce high rates of mortality, affecting the competition between microbes and the flux of resources in their environment[7]. Bacteria have evolved myriad resistance mechanisms against phage infection[8]. Because bacteria have evolved to compete with each other within ecosystems that include phages, we hypothesize that microbes may deprive their competitors of phage resistance and sensitize competitors to phages to gain a relative fitness advantage. A similar form of 'weaponizing' phages has been reported in which the secretion of secondary metabolites by one bacterial species induces lysogenic phages to become lytic and kill the host of another species[9–11]. Otherwise, most cases report that secondary metabolites protect bacteria from phages[12]. To identify instances where a microbe sensitizes competing bacteria to phages, we screened soil bacteria for isolates that improved the infectivity of bacteriophages on the model soil bacterium *Bacillus subtilis*.

We discovered that a *Streptomyces* sp. outcompetes *B. subtilis* in laboratory culture by secreting a metabolite that sensitizes *B. subtilis* to phage infection. The metabolite is a common siderophore named coelichelin, which elicited its effect via iron sequestration. We further

[1]Department of Chemistry, Indiana University, Bloomington, IN, USA. [2]Department of Biology, Indiana University, Bloomington, IN, USA. [3]Center for Genomics and Bioinformatics, Indiana University, Bloomington, IN, USA. e-mail: jpgerdt@iu.edu

https://doi.org/10.1038/s41564-024-01910-8

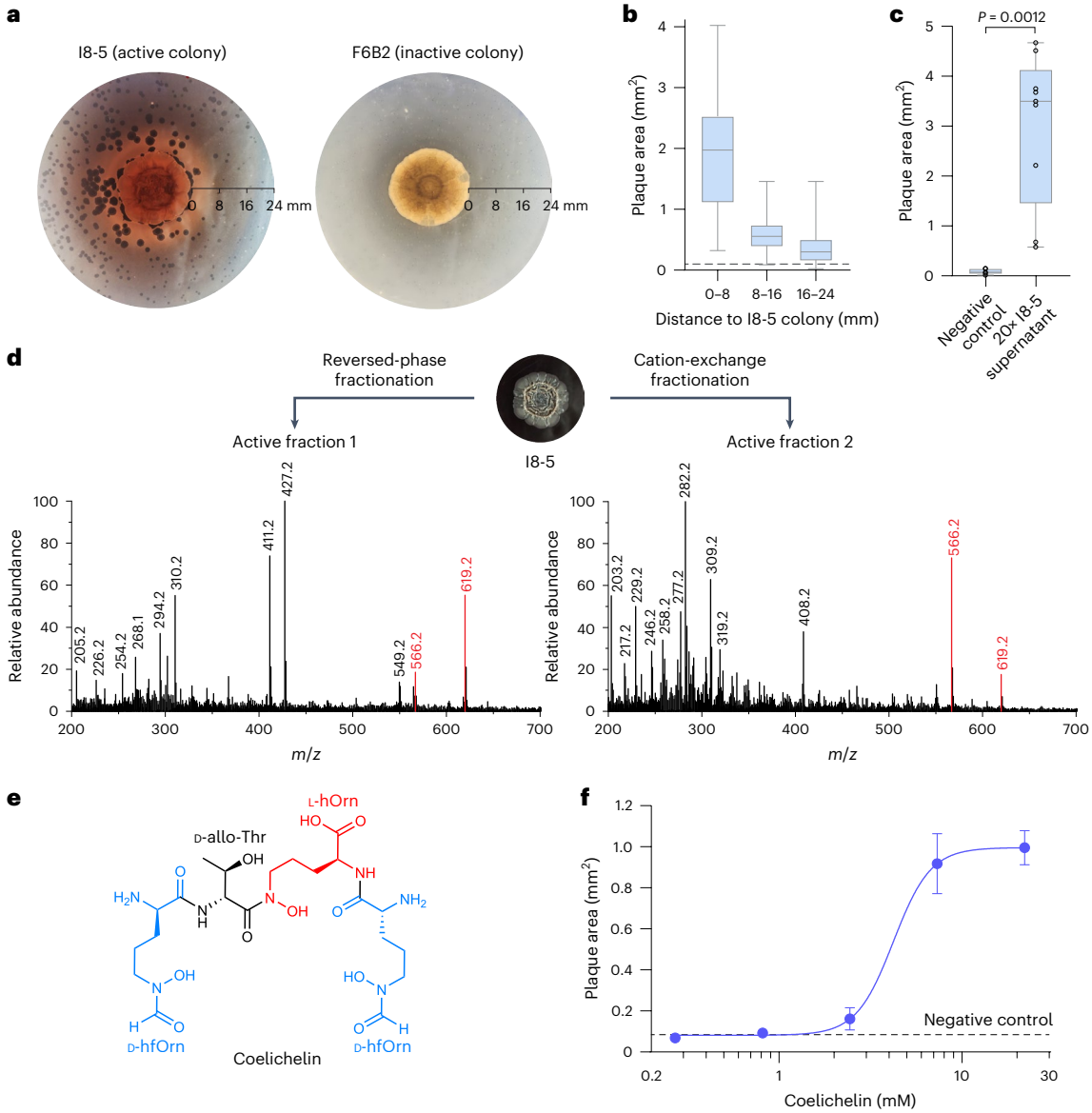

Fig. 1 | *Streptomyces* sp. produces metabolite that promotes SPO1 phage predation of *B. subtilis*. **a**, A mature colony of *Streptomyces* sp. I8-5 (centre of the plate) promoted SPO1 phage proliferation nearby (dark circles are plaques), especially within a radius of 8 mm (left). However, plaques remained small near a colony of an inactive *Streptomyces* sp. F6B2 (right). **b**, Quantification of plaque areas with increasing distance from the *Streptomyces* sp. I8-5 colony. Data are presented as boxplots, showing the median, interquartile ranges, minimum (bottom bar) and maximum (top bar). The dashed line represents the average plaque area of SPO1 phages in the absence of the *Streptomyces* colony. At least 72 plaques were measured for each condition. **c**, The I8-5 supernatant was concentrated 20 times and tested (2 µl) for the ability to enlarge SPO1 plaques. Water was used as a negative control. Data are presented as boxplots, showing the median, interquartile ranges, minimum (bottom bar) and maximum (top bar). Symbols represent individual plaque areas. At least five plaques were measured for each distance range. **d**, Bioactivity-guided fractionation and MS analysis identified two putative metabolites present in both active fractions purified from orthogonal separation techniques. Positive-mode electrospray ionization results are shown here, and matching negative-mode peaks (*m/z* 564.2 and 617.2) are shown in Extended Data Fig. 1b. **e**, Chemical structure of coelichelin, highlighting each amino acid residue. **f**, Purified coelichelin enlarged phage plaques in a dose-dependent manner (EC_{50} = 4.2 mM, 2 µl). Water was used as a negative control. Data are presented as the average ± s.e.m. of at least seven individual plaques for each condition.

found that the improved phage infection was due to the ability of coelichelin to delay the stationary phase transition of *B. subtilis*. This delay broadly sensitized *B. subtilis* to many lytic phages. Moreover, our data suggest that other bacterial metabolites beyond siderophores promote phage infectivity independently of iron. Therefore, microbes may leverage many mechanisms to sensitize neighbouring bacteria to phages, affording a phage-dependent competitive advantage.

Results

Streptomyces metabolites promote *B. subtilis* phage infection

We performed a binary-interaction screen to identify bacteria that promote phage infections in *B. subtilis*. Colonies of soil-isolated Actinomycetia were pre-grown on an agar plate to secrete metabolites into the medium (Extended Data Fig. 1a). Subsequently, *B. subtilis* and phage SPO1 were plated around the mature Actinomycetia colonies. Without an adjacent Actinomycetia colony, the SPO1 plaque sizes were small (0.11 ± 0.05 mm²). In a screen of 97 soil-derived bacteria, we found several that caused SPO1 to form larger plaques on *B. subtilis* (Supplementary Figs. 1–5). One of the clearest plaque-enlarging isolates was *Streptomyces* sp. I8-5 (Fig. 1a,b). Notably, the plaque sizes were most enlarged (1.96 ± 0.21 mm²) near the *Streptomyces* colony, and distant plaques were essentially the normal small size (Fig. 1b). This distance dependence suggested the production of a diffusible substance that promoted plaque expansion, or possibly the depletion of a diffusible plaque inhibitory substance from the media.

https://doi.org/10.1038/s41564-024-01910-8

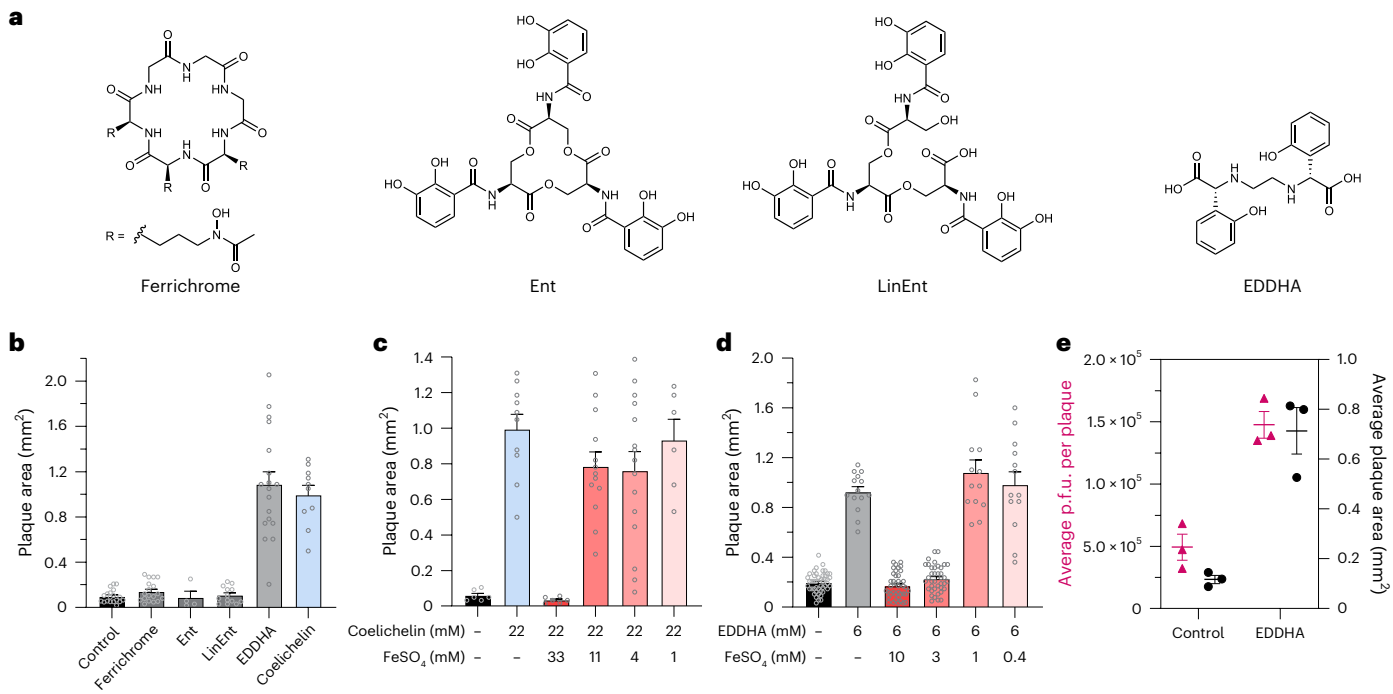

Fig. 2 | Coelichelin promotes phage predation by sequestering iron. **a**, Chemical structures of ferrichrome, enterobactin (Ent), linear enterobactin (LinEnt) and ethylenediamine-*N*,*N*′-bis(2-hydroxyphenyl-acetic acid) (EDDHA). **b**, Ferrichrome (20 mM), Ent (10 mM), LinEnt (20 mM) and EDDHA (6 mM) were tested (2 µl) for the ability to increase SPO1 plaque areas. Water was used as a negative control. Data are presented as the average ± s.e.m. of at least four individual plaques for each condition. Symbols represent individual plaque areas. **c**,**d**, Iron complementation antagonized the plaquing promotion effect of coelichelin (**c**) and EDDHA (**d**). Water was used as a negative control. Data are presented as the average ± s.e.m. of at least 6 (**c**) or 14 (**d**) individual plaques for each condition. Symbols represent individual plaque areas. **e**, The average p.f.u. per plaque (magenta triangles, left axis) and plaque area (black circles, right axis) were measured with EDDHA (6 mM, 2 µl) or water (control) treatment. Data are presented as the average ± s.e.m. of three independent biological replicates. Symbols show the values of each biological replicate. At least 13 plaques were selected for each replicate.

To investigate whether the promoted plaquing was due to metabolites secreted from the I8-5 colony, we tested the activity of sterile-filtered conditioned medium of I8-5 culture on SPO1 plaquing. Adding conditioned medium increased the plaque sizes ~30-fold (Fig. 1c), suggesting that secreted component(s) from I8-5 promote SPO1 infection on *B. subtilis*.

Phage-promoting metabolite is the siderophore coelichelin

To identify the phage-promoting metabolite(s) made by *Streptomyces* sp. I8-5, the conditioned medium of I8-5 culture was subjected to bioactivity-guided fractionation. Two active semi-pure fractions were obtained from different purification strategies: one from reversed-phase chromatography and the other from cation-exchange chromatography (Fig. 1d). Since these are relatively orthogonal separation methods, we suspected that few metabolites would be shared between the active fractions. Indeed, by liquid chromatography-mass spectrometry (LC–MS), we found that only two putative metabolites were shared by the two fractions (Fig. 1d). High-resolution mass spectrometry of these two metabolites revealed one with *m*/*z* 566.2783 and one with *m*/*z* 619.1885 (both were probably $[M+H]^+$ adducts due to matching $[M-H]^-$ adducts observed by negative-mode analysis; Extended Data Fig. 1b). The accurate mass and the tandem mass spectrometry (MS/MS) fragmentation pattern of the *m*/*z* 566.2783 species matched the known metabolite coelichelin[13] (Fig. 1e and Extended Data Fig. 1c). Because coelichelin is a siderophore with high affinity to iron[13,14], the *m*/*z* 619.1885 species was attributed to the Fe–coelichelin complex $[M-2H+Fe]^+$ with a matching MS/MS fragmentation pattern (Extended Data Fig. 1d). To confirm the ability of *Streptomyces* sp. I8-5 to produce coelichelin, we sequenced its genome and identified the coelichelin biosynthetic gene cluster (BGC) (Extended Data Fig. 1e). The coelichelin BGC in I8-5 has the same organization as the reported one with high sequence identity[13] (>75% for each gene; Extended Data Fig. 1e). Consistent with the reported coelichelin non-ribosomal peptide synthetase (NRPS)[13], epimerization domains were identified in the first and second module of the I8-5 coelichelin NRPS (Extended Data Fig. 1e). These domains suggest that the absolute stereochemistry of our analyte is the same as reported[13] (Fig. 1e).

To determine whether coelichelin was the active component secreted by *Streptomyces* sp. I8-5, we purified coelichelin from the *Streptomyces*-conditioned medium (Extended Data Fig. 2). Nuclear magnetic resonance (NMR) analyses confirmed the identity and purity of our isolated coelichelin (Supplementary Figs. 6–10 and Supplementary Table 1). As hypothesized, the purified coelichelin enlarged plaques in a dose-dependent manner, confirming that it is a phage-promoting metabolite secreted by *Streptomyces* sp. I8-5 (Fig. 1f).

Coelichelin promotes phage proliferation by iron sequestration

Since coelichelin is a hydroxamate-type siderophore[13–16], we hypothesized that other siderophores would also enlarge plaques of SPO1. We tested three other common siderophores: ferrichrome, enterobactin and linear enterobactin (Fig. 2a). Surprisingly, none of these siderophores increased plaque size (Fig. 2b). Previous work has demonstrated that *B. subtilis* can import a range of xenosiderophores produced by other organisms (in addition to using its own siderophore bacillibactin)[17]. This list of 'pirated' siderophores notably includes all three that failed to enlarge plaques[18–20]. Therefore, we hypothesized that only siderophores that cannot be imported and utilized by *B. subtilis* enlarge plaques. The non-usable siderophores would sequester iron away from *B. subtilis* and, via an unknown mechanism, improve phage replication on the iron-starved host.

It was previously unknown whether coelichelin could sequester iron away from *B. subtilis* (or whether *B. subtilis* could instead use it as a xenosiderophore). Therefore, to test the iron sequestration hypothesis, we utilized a synthetic iron chelator, EDDHA (Fig. 2a), which is known to sequester iron away from *B. subtilis*[21]. In line with our hypothesis, EDDHA increased SPO1 plaque sizes to a similar level as coelichelin (Fig. 2b). Furthermore, if iron starvation was responsible for the improved plaquing, the plaque sizes should decrease to their normal size when excess iron is co-administered with the siderophore. As expected, approximately equimolar concentrations of $FeSO_4$ quenched the plaque-enlarging effect of both coelichelin and EDDHA (Fig. 2c,d). We hypothesized that the enlarged plaques were the result of increased phage proliferation within each plaque. To test this hypothesis, we quantified the viable phages (plaque-forming units (p.f.u.)) generated per plaque. Indeed, the larger plaques afforded by iron limitation produced more phages (Fig. 2e). Thus, we concluded that *B. subtilis* does not use coelichelin as a xenosiderophore. Furthermore, the iron starvation caused by this *Streptomyces* siderophore promotes the predation of *B. subtilis* by SPO1 phages.

Phage infection is promoted by inhibition of Spo0A activation

We next investigated the mechanism by which iron starvation promoted phage infection in *B. subtilis*. Plaque size can be increased by many factors that either accelerate the rate of phage replication or extend the period in which phages can replicate before the bacteria becomes recalcitrant. For example, the rate of plaque expansion depends largely on the burst size (that is, the number of new phages released from each infected cell) and latent period (that is, the time required for phages to lyse the host cell and produce new progeny) of phage replication. Specifically, large burst sizes and shorter latent periods maximize the phage reproduction rate, thus resulting in larger plaques[22]. We considered whether iron starvation increased burst size and/or shortened the latent period of phage replication. It has been reported that iron starvation actually has the opposite effect in *Vibrio cholerae*: it reduces burst size and delays phage-mediated cell lysis[23]. In line with the *V. cholerae* study, we observed that when *B. subtilis* grew next to *Streptomyces* sp. I8-5, the plaque development of SPO1 was slower than plaque development alone, suggesting that iron sequestration does not accelerate phage replication (Fig. 3a). However, we observed that the plaque development process lasted longer in the presence of the *Streptomyces* colony, leading to larger plaques (Fig. 3a). This longer plaque development (in combination with higher p.f.u. production in larger plaques; Fig. 2e) indicated that phages underwent more reproduction cycles, lysing more *B. subtilis* cells and ultimately forming 10× larger plaque areas.

The extended period of phage infection led us to consider an alternative mechanism: iron starvation may interfere with host dormancy. Reproduction and plaque development by many phages is optimal on metabolically active host cells[24–27]. Under suboptimal conditions, many bacteria enter dormant stages with heavily reduced metabolic activity[28], which is typically unfavourable for phage proliferation. Therefore, dormancy can be considered a mechanism of phage resistance. In *B. subtilis*, nutrient starvation and other stresses lead to the activation of the transcriptional master regulator Spo0A, which triggers a transition from vegetative exponential growth to stationary phase and eventually, sporulation[29]. To test the hypothesis that Spo0A activation could repress phage infection, we examined plaque formation on *B. subtilis* strains encoding IPTG-inducible sad67-D56N, which is a mutant form of Spo0A 'locked' in its active state[30]. When the active Spo0A (sad67-D56N) was expressed under IPTG induction, the plaque formation of SPO1 was restricted (Fig. 3b). Therefore, transition into stationary phase and/or sporulation prevents plaque enlargement in *B. subtilis* (Fig. 3c).

Since two Spo0A-activated stationary phase phenotypes (biofilm formation and sporulation) in *B. subtilis* rely on sufficient levels of intracellular iron[31,32], we asked whether iron sequestration could prevent Spo0A-induced transition into stationary phase and maintain *B. subtilis* in the phage-susceptible vegetative growth state (Fig. 3c). To test this hypothesis, we first determined whether iron sequestration prevented the activation of Spo0A under our experimental conditions by quantifying the formation of *B. subtilis* spores. We found that both coelichelin and EDDHA inhibited sporulation (Spo0A activation) in *B. subtilis* (Fig. 3d). This inhibitory effect was due to iron sequestration, as demonstrated by the ability of iron supplementation to recover native levels of sporulation (Fig. 3d).

To further determine whether the cause of increased phage proliferation was inhibition of Spo0A activation, we employed a knockout mutant of *B. subtilis spo0A*, which is incapable of entering stationary phase and thus 'locked' in its vegetative growth state[33,34]. We predicted that this mutant would naturally form large plaques that are not further enlarged by iron limitation. Indeed, the SPO1 phage formed extremely large plaques on the Δ*spo0A* mutant (Fig. 3e). As expected, the mutant plaques were not enlarged by EDDHA-induced iron sequestration. In fact, the plaques were substantially smaller under EDDHA treatment, possibly due to impeded phage proliferation under iron limitation, similar to what we have observed with *V. cholerae*[23]. A nearly identical phenotype was observed for the mutants Δ*spo0F* and Δ*spo0B*, which are part of the phosphorelay that activates Spo0A[35] (Fig. 3e,f), providing more evidence that iron sequestration enlarges plaques by inhibiting the activation of Spo0A (Fig. 3f). Therefore, our results demonstrate that iron sequestration extends phage infection on *B. subtilis* by inhibiting the activation of Spo0A, the master regulator of the stationary phase and sporulation.

Plaque enlargement is due to multiple Spo0A-regulated pathways

Sporulation has been shown to restrict plaque development[36] by masking surface receptors[37]. Therefore, we hypothesized that our observed plaque enlargement (by inhibiting Spo0A activation) was due to inhibited sporulation. To test this hypothesis, we examined three sporulation genes regulated by Spo0A (Extended Data Fig. 3a): *spoIIAA*, *sigF* and *spoIIE* (the earliest known sporulation-specific regulator[38]). If inhibiting sporulation was the mechanism of plaque enlargement, we would expect these mutants to phenocopy the Δ*spo0A* mutant (large plaques that are not enlarged by iron limitation). However, the plaques in these mutants were as small as those in the wild type (WT) and were significantly enlarged by iron sequestration (Extended Data Fig. 3b). Therefore, sporulation is 'not' essential to the observed Spo0A-induced plaque restriction under our experimental conditions.

Before *B. subtilis* commits to sporulation, Spo0A activates many other pathways in *B. subtilis* during the transition from exponential growth to the stationary phase[29] (Fig. 3f). These pathways include decreasing motility, increasing biofilm formation, increasing competence, increasing cannibalism, decreasing translation and amino acid metabolism, and decreasing nucleotide metabolism[29,34]. All of these responses (perhaps except for increased competence) could intuitively inhibit phage reproduction and decrease plaque sizes[24–27,39]. Most of these pathways were regulated by two parallel pathways of repression mediated by SinI/SinR and AbrB[40] (Extended Data Fig. 3a). To test whether SinI/SinR or AbrB were important for plaque restriction, we investigated three mutants: Δ*sinI*, Δ*spo0A*Δ*sinR* and Δ*spo0A*Δ*abrB* (Extended Data Fig. 3b). We observed that the Δ*sinI* mutant was able to generate slightly larger plaques, and iron sequestration marginally enlarged plaques. We also found that deletion of either *abrB* or *sinR* from the Δ*spo0A* background each partially (but incompletely) abrogated the enlarged-plaque phenotype of Δ*spo0A*. Therefore, both SinI/SinR and AbrB appear to be partially responsible for plaque restriction by Spo0A activation. To further dissect which pathways regulated by SinI/SinR and AbrB were important for the plaque restriction, we examined mutants of each pathway.

https://doi.org/10.1038/s41564-024-01910-8

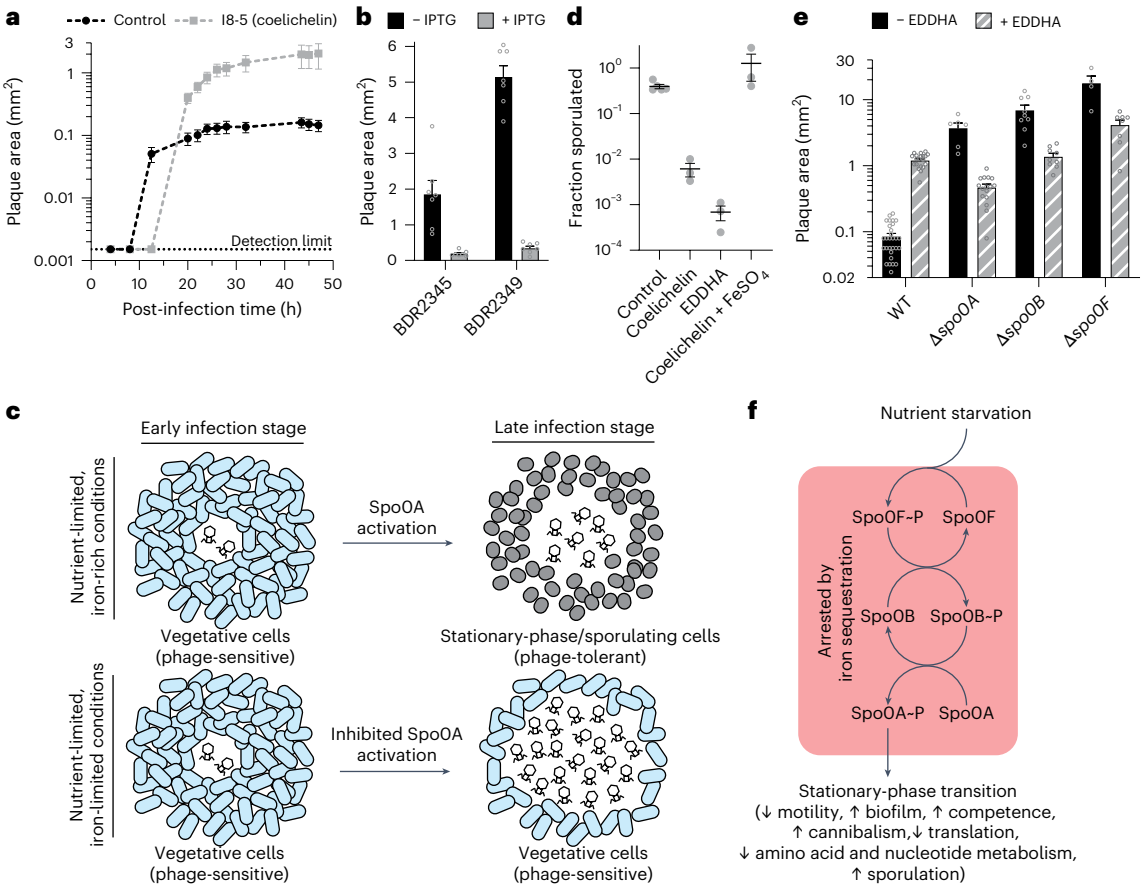

Fig. 3 | Iron sequestration inhibits SpoOA activation in *B. subtilis*. **a**, Plaque size development of SPO1 phage on *B. subtilis* grown ~8 mm away from an I8-5 colony (coelichelin producer) or *B. subtilis* alone (control). Data are presented as the average ± s.e.m. of at least eight individual plaques for each condition. **b**, IPTG-induced expression of SpoOA (sad67-D56N) restricted phage infection in *B. subtilis* strains BDR2345 and BDR2349. Data are presented as the average ± s.e.m. of at least seven individual plaques for each condition. Symbols represent individual plaque areas. **c**, Schematic model for iron sequestration-induced promotion of phage infection: under iron-rich conditions, *B. subtilis* cells enter stationary phase and eventually sporulate when nutrients are limited. Once the stationary-phase transition occurs in *B. subtilis* cells, phage proliferation is diminished (top). However, when iron is limited, the transition into stationary phase (and eventually sporulation) is delayed, allowing phages to continue infecting vegetative *B. subtilis* cells (bottom). **d**, Influence of iron starvation on *B. subtilis* sporulation. The fraction of *B. subtilis* cells that sporulated under treatment (2 µl) of water (control), coelichelin (22 mM), EDDHA (6 mM) and coelichelin (22 mM) + $FeSO_4$ (33 mM). Iron starvation inhibited sporulation. Data are presented as the average ± s.e.m. of three independent biological replicates. Circles show the values of each biological replicate. **e**, The plaque-enlarging effect of EDDHA (6 mM, 2 µl) was tested against *B. subtilis* WT, Δ*spoOA*, Δ*spoOB* and Δ*spoOF*. Water was used as the −EDDHA control. The Δ*spoOA*, Δ*spoOB* and Δ*spoOF* mutants naturally formed larger plaques that were not further increased by iron sequestration. Data are presented as the average ± s.e.m. of at least four individual plaques for each condition. Symbols represent individual plaque areas. **f**, Schematic representation of the phosphorelay that activates SpoOA and downstream pathways in *B. subtilis*.

First, we investigated motility and biofilm formation. Activation of SpoOA switches *B. subtilis* from a motile cell to a sessile biofilm through parallel regulation by SinI/SinR and AbrB[40] (Extended Data Fig. 3a). Since motile cells may disperse phages more rapidly and biofilms may inhibit the diffusion of phages, this switch could constrict plaque sizes[39]. Inhibition of these processes would thus enlarge plaques. We note that our model strain of *B. subtilis* is a 168 derivative, which is already deficient in motility and biofilm formation[41]. Nonetheless, we examined multiple mutants in motility (Δ*sigD*, Δ*hag*, Δ*motA*) and biofilm formation (Δ*epsE*, Δ*tasA*, Δ*yuaB*). All of the mutants showed the same phenotype as the WT strain (Extended Data Fig. 3b). Therefore, no individual biofilm or motility gene was necessary for the SpoOA-induced plaque restriction. However, a combination of them may still be required.

Then we investigated competence and cannibalism in *B. subtilis*, which are regulated by the AbrB pathway (Extended Data Fig. 3a). We first examined ComK, the key regulatory protein for competence development in *B. subtilis*[42]. However, inhibition of competence (Δ*comK*; Extended Data Fig. 3b) exhibited the same phenotype as WT, suggesting that competence is not important for SpoOA-induced plaque restriction. We next examined the cannibalism pathway that delays the commitment of the *B. subtilis* population to sporulation. Due to the heterogeneity of SpoOA activation in the *B. subtilis* population, the two cannibalism toxins (Skf and Sdp) expressed by cells with activated SpoOA (SpoOA~P) kill neighbouring cells with unphosphorylated SpoOA[43,44]. Since vegetative cells with unphosphorylated SpoOA are the ideal host for phage propagation, we hypothesized that the production of Skf and Sdp toxins could maintain a population of *B. subtilis* solely with activated SpoOA, which would restrict plaque development. To test this hypothesis, we generated a double knockout mutant Δ*skfA*Δ*sdpC* that cannot produce these toxins. Indeed, the Δ*skfA*Δ*sdpC* mutant partially reproduced the phenotype of the Δ*spoOA*Δ*abrB* mutant (Extended Data Fig. 3b), suggesting that cannibalism may play a role in SpoOA/AbrB-activated plaque restriction.

From these analyses of several mutants, no single SpoOA-regulated phenotype was sufficient to completely explain the importance of SpoOA activation for plaque restriction. It is possible that multiple pathways may act synergistically to restrict plaque size. In addition,

https://doi.org/10.1038/s41564-024-01910-8

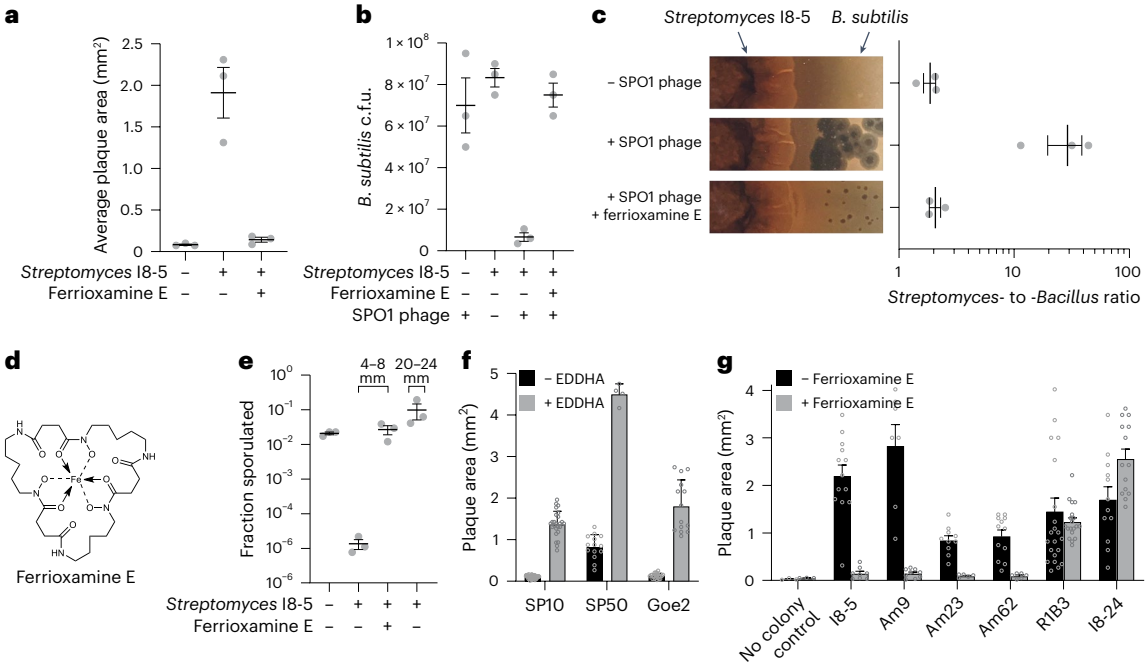

Fig. 4 | Phage-promoting metabolites help producers to outcompete *B. subtilis*. **a**, The average plaque areas of SPO1 on *B. subtilis* alone and *B. subtilis* neighbouring *Streptomyces* I8-5 colony with or without ferrioxamine E (20 mM, 2 µl) as an excess iron source. Data are presented as the average ± s.e.m. of three independent biological replicates. Circles show the values of each biological replicate. At least eight plaques were selected for each replicate. **b**, Colony-forming units (c.f.u.) of *B. subtilis* measured when infected by phages, neighbouring *Streptomyces* I8-5 colony, and in a combination of phage and I8-5 with or without ferrioxamine E as excess iron source. Data are presented as the average ± s.e.m. of three independent biological replicates. Circles show the values of each biological replicate. **c**, *Streptomyces* to *B. subtilis* ratio calculated from c.f.u. measured after 2 days of co-culture. Data are presented as the average ± s.e.m. of three independent biological replicates. Circles show the values of each biological replicate. **d**, The chemical structure of ferrioxamine E. **e**, The impact of the *Streptomyces* I8-5 colony on *B. subtilis* sporulation (an indicator of Spo0A activation). The distance of *B. subtilis* to the *Streptomyces* colony is indicated at the top. Data are presented as the average ± s.e.m. of three independent biological replicates. Circles show the values of each biological replicate. **f**, The plaque-enlarging effect of EDDHA (6 mM, 2 µl) for phages SP10, SP50 and Goe2 on *B. subtilis*. Water was used as the −EDDHA control. Data are presented as the average ratio ± s.e.m. calculated from at least four individual plaques for each condition. Symbols represent individual plaque areas. **g**, The plaque-enlarging effect of five other soil Actinomycetia. *B. subtilis* SPO1 plaque size was measured 4–8 mm away from the Actinomycetia. If addition of ferrioxamine E to the *B. subtilis*/SPO1 overcame the plaque enlargement, it would suggest that the phage metabolites produced by the Actinomycetia were siderophores. Data are presented as the average ratio ± s.e.m. calculated from at least three individual plaques for each condition. Symbols represent individual plaque areas.

the general decrease in ribosome number and amino acid and nucleotide metabolism in Spo0A-activated cells[34] may slow the progress of phage replication.

In conclusion, our analysis of plaquing in mutant *B. subtilis* strains suggests that multiple Spo0A-regulated pathways may redundantly restrict phage replication and decrease plaque sizes. Iron sequestration inhibits the activation of Spo0A, releasing these restrictions to allow continued phage propagation and enlarged plaques in *B. subtilis*.

Streptomyces outcompetes *B. subtilis* in a coelichelin- and phage-dependent manner

B. subtilis and *Streptomyces* are both soil bacteria and are likely to share habitats in nature[45]. Since coelichelin secreted by *Streptomyces* sp. I8-5 promoted phage infection on *B. subtilis* (Fig. 4a), we hypothesized that coelichelin offers *Streptomyces* a competitive advantage over *B. subtilis* in the presence of *Bacillus* phages. Indeed, the combined action of SPO1 phages and a nearby *Streptomyces* sp. I8-5 colony significantly decreased the *B. subtilis* population density relative to phage treatment or *Streptomyces* treatment alone (Fig. 4b). Importantly, this effect allowed *Streptomyces* to outcompete *B. subtilis* 15:1 under our growth conditions (Fig. 4c).

To validate the importance of coelichelin-induced iron sequestration for the decreased *B. subtilis* fitness, we supplied the *B. subtilis* cells with excess bioavailable iron in the form of a xenosiderophore–iron complex, ferrioxamine E (Fig. 4d). With ferrioxamine E as a supplemented iron source, the phage promotion effect from *Streptomyces* was abolished and *Streptomyces* lost its phage-induced competitive advantage over *B. subtilis* (Fig. 4a–c and Extended Data Fig. 4). We note that this experiment does not conclusively show the necessity of *coelichelin* per se. A second iron-sequestering metabolite could conceivably play a complementary role. Nonetheless, this experiment demonstrates that secretion of iron-sequestering metabolites enables *Streptomyces* sp. I8-5 to outcompete *B. subtilis* by facilitating phage predation on its competitor.

Furthermore, we hypothesized earlier that iron sequestration promoted phage infection by inhibiting the activation of Spo0A. Using sporulation as a proxy for Spo0A activation, we verified that the I8-5 colony inhibited sporulation of nearby *B. subtilis* (Fig. 4e). Just as the *Streptomyces* colony's impact on increased phage killing was quenched by bioavailable iron (+ferrioxamine E), so too was the colony's ability to inhibit sporulation (that is, inhibit Spo0A activation) (Fig. 4e). We also observed matching distance dependence from the *Streptomyces* colony for both plaque enlargement (Fig. 1b) and inhibition of sporulation (that is, inhibition of Spo0A activation) (Fig. 4e). This observed correlation between increased plaque sizes, increased relative fitness of *Streptomyces* and decreased *B. subtilis* sporulation (that is, decreased Spo0A activation) supports our model that siderophores from *Streptomyces* sp. I8-5 can confer a competitive advantage to their producer by sensitizing neighbouring *B. subtilis* to phage infection via inhibiting Spo0A activation.

Diverse competitors sensitize *B. subtilis* to multiple phages

Finally, we asked how widespread this metabolite-induced phage sensitization could be. We aimed to determine whether the effect was limited to the SPO1 phage and the *Streptomyces* sp. I8-5, or instead, whether a range of phages exhibit enlarged plaques in response to a range of microbial metabolites. We tested three other *Bacillus* phages (SP10, SP50 and Goe2)[46,47], and found that the virulence of all three was substantially increased by iron sequestration (Fig. 4f). Then we examined five of the other unique strains (Am9, Am23, Am62, R1B3, I8-24; Supplementary Figs. 1–5) in our library that also enlarged plaque sizes of SPO1 on *B. subtilis* in our initial screen (Fig. 4g). In three of the five strains, the effect was quenched by the addition of bioavailable iron, suggesting the same mechanism—secretion of iron-chelating metabolites (Fig. 4g). Coelichelin itself was not detected in the supernatant of the Am23 culture (Extended Data Fig. 5), suggesting that other siderophores may also be capable of enlarging plaques. Notably, the phage-promoting effects of R1B3 and I8-24 were independent of iron. This discovery suggests that beyond siderophores, other metabolites can also sensitize competitors to phage infections. Therefore, secondary metabolites produced by many competing microbes may broadly sensitize *B. subtilis* to a variety of phages in nature.

Discussion

We discovered that a bacterial strain gains competitive advantage over neighbouring bacteria by producing a secondary metabolite that sensitizes its competitor to phage predation. In our culture conditions, the metabolite–phage synergy switched the outcome of the bacterial competition to strongly favour the metabolite producer. Our discovery adds to the small but growing number of microbial natural products that influence bacteriophage infection, either by inhibiting phage proliferation[12], promoting phage proliferation[48], or triggering the lytic phase of lysogenic phages[9–11]. We isolated the active metabolite, the known siderophore coelichelin. We further posited that this metabolite sequestered iron away from *B. subtilis* and promoted phage infection by inhibiting Spo0A activation. This finding reveals a new mechanism by which siderophores can shape microbial competition through bacteria–phage ecology.

Siderophores are primarily believed to enable their producer to acquire essential iron ions[5,16]. Beyond iron acquisition, siderophores can also benefit their producers by starving competing microbes of iron[5,49]. Our results further show that siderophores can block the stationary phase transition and sporulation of competing bacteria, which could be beneficial for the siderophore producer in fluctuating environments. For example, by excluding spores of a competitor, the siderophore-producer's spores would revive without competition when conditions become optimal for germination[50–52] Finally, our work reveals a potential fourth benefit of siderophore production: microbes can sensitize competing bacteria to lytic phages. This phage-promoting effect may benefit the multitude of siderophore-producing bacteria and fungi[16] that compete with *B. subtilis* and its relatives.

Although our studies focused on soil *Streptomyces* and the model soil bacterium *B. subtilis*, Spo0A-regulated dormancy behaviours are characteristic of many bacteria in the Bacillota (Firmicutes) phylum[53]. These bacteria are not only abundant in soil and aquatic sediments, but they are also important members of host-associated microbiomes, including some common intestinal pathogens and mutualistic taxa in humans[54]. Therefore, it is plausible that secondary metabolites sensitize diverse Bacillota (Firmicutes) in varied environments to phage infection by inhibiting the stationary phase transition. In fact, secondary metabolites other than siderophores have also been shown to inhibit Spo0A activation or expression in Bacillota. For example, a common signal molecule used for quorum sensing, autoinducer-2, inhibits Spo0A activation in *Bacillus velezensis*[55]. Furthermore, the bacterial macrocycle fidaxomicin inhibits *spo0A* gene expression in *Clostridioides difficile*[56]. Beyond microbe–microbe competition, multicellular hosts may also sensitize resident bacteria to lytic phages by producing iron-sequestering proteins[57] or other molecules that may inhibit Spo0A. Therefore, microbial siderophores, other microbial secondary metabolites and even host-produced molecules may sensitize competing bacteria to phage infection in natural communities.

In conclusion, we discovered a case in which a natural product, coelichelin, gives its producer an advantage by sensitizing its competitors to phages. Despite a rich history of studies on the 'chemical warfare' waged between microbes via natural products, little emphasis has been placed on how phage predation intersects with microbial secondary metabolites. This work reveals that microbial natural products do not just directly inhibit the fitness of microbial competitors, but these molecules can also sensitize competitors to lytic phages. Although the extent of this phenomenon in nature is yet to be seen, it may shape the microbial ecology of both environmental and host-associated ecosystems. Also, much like society has leveraged microbial competition to discover life-saving antimicrobials, phage-promoting natural products may also prove useful one day as co-administered adjuvants in phage-based interventions.

Methods

Strains and growth conditions

The strains and bacteriophages used in this study are listed in Supplementary Tables 2 and 3. All chemicals used are listed in Supplementary Table 4. All primers used are listed in Supplementary Table 5. *B. subtilis* strains were routinely grown in LB broth at 37 °C and 220 r.p.m. When appropriate, antibiotics were used at the following concentrations: 7 μg ml^{-1} kanamycin and 1 μg ml^{-1} erythromycin. *Streptomyces* strains were routinely grown in ISP2 media (4 g l^{-1} yeast extract, 10 g l^{-1} malt extract and 4 g l^{-1} dextrose) at 30 °C and 220 r.p.m.

Bacteriophage lysate preparation

To prepare the host culture, an overnight culture of *B. subtilis* RM125 WT was subcultured 1:100 into 4 ml LB + 0.1 mM $MnCl_2$ + 5 mM $MgCl_2$ + 5 mM $CaCl_2$. The culture was incubated at 37 °C and 220 r.p.m. for 4 h until the optical density $(OD)_{600nm}$ reached 0.2. About 1×10^3 plaque-forming units (p.f.u.) of *Bacillus* phage were added to the culture. The phage-infected culture was incubated at 37 °C and 220 r.p.m. until bacterial cells were lysed and the culture turned clear. The phage lysate was filtered through a 0.2-μm polyethersulfone filter and stored at 4 °C.

Binary-interaction screening

To prepare plates with library bacteria, 5 μl of the frozen spore stock of each bacterial strain in our library was suspended in 50 μl of ISP2 medium. Then 8 μl of the spore suspension was spotted at the centre of an ISP2 + 1.5% agar plate. The inoculated plates were incubated at 30 °C for 10 days to allow the library bacteria to grow and secrete their metabolites into the plate. To test the influence of the metabolites on phage infectivity, an overnight culture of *B. subtilis* RM125 WT was diluted 1:10 into 5 ml fresh LB broth and ~1,000 p.f.u. of SPO1 phages was then added into the medium. The mixture of bacteria and phages was poured around the central colony formed by the library bacteria. Bacteria and phages were allowed 10 min to soak the plate and the mixture was then removed using a pipette. The plate was dried under room temperature in a biosafety cabinet and then incubated at 37 °C overnight. The size of plaques formed by SPO1 was quantified using Fiji[58] the next day.

16S ribosomal RNA sequencing of Actinomycetia

A single colony of Actinomycetia was inoculated into 4 ml fresh ISP2 medium and incubated at 30 °C and 220 r.p.m. for 4 days. The genomic DNA was extracted from 1 ml liquid mycelia culture using Promega Wizard Genomic DNA Purification kit (1120). The 16S ribosomal RNA (rRNA) region of the bacterial genome was amplified by PCR using

16S_F and 16S_R primers. Sanger sequencing results of 16S rRNA are available on NCBI (I8-5: GenBank OR902106; Am9: GenBank PQ178887; Am23: GenBank PQ178944; Am62: GenBank PQ178965; R1B3: GenBank PQ178995; I8-24: GenBank PQ179041).

Coelichelin biosynthetic gene cluster identification in I8-5

The library of the extracted genomic DNA was prepared using the Illumina Nextera XT DNA Library Prep Kit protocol (FC-131-1096) and analysed using Agilent D1000 ScreenTape. The libraries were pooled and loaded on a NextSeq 1000/2000 P2 Reagents (100-cycles) v3 flow cell (20046811) configured to generate paired-end reads. The demultiplexing of the reads was performed using bcl2fastq v.2.20.0. Reads were adapter trimmed and quality filtered using Trimmomatic (0.38)[59] with the cut-off threshold for average base quality score set at 20 over a window of 3 bases requiring a minimum trimmed read length of 20 bases (parameters: LEADING:20 TRAILING:20 SLIDINGWINDOW:3:20 MINLEN:20). The cleaned reads were assembled using SPAdes (v.3.15.4)[60] with default parameters. The assembly was annotated using prokka (v.1.12)[61], employing a sequence training set prepared from protein sequences obtained from 431 publicly available *Streptomyces* assemblies (parameters: --minpid 70 --usegenus --hmmlist TIGRFAM,CLUSTERS,Pfam,HAMAP). The coelichelin biosynthetic gene cluster was identified using antiSMASH (7.0)[62]. The genomic sequences are available on NCBI (accession number: JAYMFC000000000).

Collection of I8-5 supernatant

To revive the spores of I8-5, 5 µl of the I8-5 frozen spore stock was streaked out on an ISP2 + 1.5% agar plate. The plate was incubated at 30 °C for 3 days until colonies formed. A single colony was inoculated into 4 ml fresh ISP2 medium and incubated at 30 °C and 220 r.p.m. for 4 days. After the incubation, 1 ml of the culture was added into 1 l of ISP2 medium and grown for another 11 days to allow metabolite production. To collect the metabolites in the supernatant, the bacteria cells in the culture were pelleted at 4,820 × *g* for 20 min and and the pellet was discarded. The supernatant was lyophilised and stored at −20 °C until ready to use.

Test of phage promotion activity of compounds/supernatant concentrate

An overnight culture of *B. subtilis* RM125 WT was diluted 1:10 into 5 ml fresh ISP2 + 0.1 mM $MnCl_2$ + 5 mM $MgCl_2$, and poured onto an ISP2 + 0.1 mM $MnCl_2$ + 5 mM $MgCl_2$ + 1.5% agar plate. Bacteria were allowed 10 min to attach to the plate and the unattached bacteria were then removed. The plate was dried under room temperature in a biosafety cabinet. To test the phage promotion effect, 2 µl of compound/supernatant concentrate was spotted on top of the bacterial lawn. After the compound dried, the plate was incubated at 37 °C for 1 h. Then 5 µl of SPO1 phage lysate (~10 p.f.u.) was spotted on top of the compound-treated area. After the phage lysate dried, the plate was incubated at 37 °C and the size of plaques formed by SPO1 was quantified using Fiji[58] after 2 days.

Fractionation of I8-5 supernatant using reversed-phase chromatography

The lyophilised supernatant was dissolved into a small amount of water as a concentrated sample. The concentrated supernatant was further separated on a Phenomenex Synergi 4 µm Hydro-RP 80 Å column (250 × 10 mm) using an Agilent 1260 Infinity II HPLC system. Mobile phase A was water + 0.01% (v/v) formic acid and mobile phase B was acetonitrile + 0.01% (v/v) formic acid. The flow rate was kept at 3 ml min^{-1} and the gradient was as follows: 0% B (0–5 min), increase to 20% B (5–6 min), 20% B for (6–11 min), increase to 80% B (11–31 min), increase to 100% B (31–32 min), 100% B (32–37 min), decrease to 0% B (37–38 min), 0% B (38–43 min). Eluted fractions were collected every 30 s and dried in vacuo. Each dried fraction was redissolved into 2 µl DMSO and spotted on a lawn of *B. subtilis* RM125 WT infected by SPO1 phages to test the phage promotion activity. The fraction eluting at 12.0–12.5 min was active and labelled as 'active fraction 1'. The composition of 'active fraction 1' was analysed on a Phenomenex Synergi 4 µm Hydro-RP 80 Å column (250 × 4.6 mm) using an Agilent 1260 Infinity II HPLC system coupled to an Agilent InfinityLab LC/MSD XT mass spectrometer. The analysis was performed at a flow rate of 0.7 ml min^{-1}. The mobile phase and separation gradient were the same as described above.

Fractionation of I8-5 supernatant using cation-exchange and reversed-phase chromatography

The lyophilised supernatant was dissolved into 10 ml 2% (v/v) formic acid/water (pH 2.02). The supernatant was loaded on a Waters Oasis MCX column (186000255). The column was then eluted with water + 2% (v/v) formic acid, methanol and methanol + 5% (v/v) ammonium hydroxide. The eluates were dried in vacuo and redissolved into water as a 100 mg ml^{-1} solution. Of each redissolved fraction, 2 µl was spotted on a lawn of *B. subtilis* RM125 WT infected by SPO1 phages to test the phage promotion activity. The methanol + 5% (v/v) ammonium hydroxide eluate was active and subjected to separation on a Phenomenex Synergi 4 µm Hydro-RP 80 Å column (250 × 10 mm) using an Agilent 1260 Infinity II HPLC system. Mobile phase A was water + 0.1% (v/v) formic acid and mobile phase B was acetonitrile + 0.1% (v/v) formic acid. The flow rate was kept at 3 ml min^{-1} and the gradient was as follows: 10% B (0–10 min), increase to 50% B (10–30 min), increase to 100% B (30–31 min), 100% B (31–38 min), decrease to 10% B (38–39 min), 10% B (39–44 min). Eluted fractions were collected every 30 s and dried in vacuo. Each dried fraction was redissolved into 2 µl DMSO and tested for phage promotion effect as described above. The fraction eluting at 3.5–4.0 min was active and labelled as 'active fraction 2'. The composition of 'active fraction 2' was analysed on a Phenomenex Synergi 4 µm Hydro-RP 80 Å column (250 × 4.6 mm) using an Agilent 1260 Infinity II HPLC system coupled to an Agilent InfinityLab LC/MSD XT mass spectrometer. The analysis was performed at a flow rate of 0.7 ml min^{-1}. The mobile phase and separation gradient were the same as described above.

LC–MS/MS analysis of *m/z* 566.2783 and *m/z* 619.1885 species

The 'active fraction 2' was separated on a Phenomenex Synergi 4 µm Hydro-RP 80 Å column (250 × 4.6 mm) using ACQUITY UPLC I-Class PLUS System. Mobile phase A was water + 0.1% (v/v) formic acid and mobile phase B was acetonitrile + 0.1% (v/v) formic acid. The flow rate was kept at 0.7 ml min^{-1} and the gradient was as follows: 0% B (0–20 min), increase to 20% B (20–21 min), increase to 40% B (21–31 min), increase to 100% B (31–32 min), 100% B (32–42 min), decrease to 0% B (42–43 min), 0% B (43–48 min). *m/z* 566.2783 species eluted at 17.2–18.2 min and *m/z* 619.1885 species eluted at 26.0–26.1 min. High-resolution electrospray ionization (HR-ESI) mass spectra with collision-induced dissociation (CID) MS/MS were obtained using a Waters Synapt G2S QTOF. Data-dependent acquisition was employed to fragment the top three masses in each scan. The data were analysed using MassLynx 4.1 software.

Isolation of coelichelin from I8-5 supernatant

The protocol was adapted from ref. 13. The lyophilised I8-5 supernatant (1.8533 g) was dissolved in 5 ml of water. $FeCl_3$ was added to the supernatant (final concentration 40 mM) to generate an Fe–coelichelin complex. The reaction mixture was centrifuged at 16,000 × *g* for 5 min and the precipitates were discarded. The supernatant was separated on a Phenomenex Luna 10 µm Hydro-RP 100 Å column (250 × 21.2 mm) using an Agilent 1260 Infinity II HPLC system. Mobile phase A was water + 10 mM NH_4HCO_3 (pH 8.01) and mobile phase B was methanol. The flow rate was kept at 10 ml min^{-1} and the gradient was as follows: 5% B (0–20 min), increase to 90% B (20–21 min), 90% B (21–31 min),

decrease to 5% B (31–32 min), 5% B (32–42 min). Fe–coelichelin eluted at 9.1–10.4 min and was collected by monitoring the absorbance at 435 nm. The collected Fe–coelichelin was concentrated in vacuo, lyophilised and obtained as an orange solid.

The obtained Fe–coelichelin (45.9 mg) was dissolved into 74 ml of water. The ferric iron was removed from the Fe–coelichelin complex by mixing the Fe–coelichelin solution with 74 ml of 100 mM 8-hydroxyquinoline in methanol. The reaction was stirred for 30 min at room temperature. The Fe–8-hydroxyquinoline complex was removed by extracting the aqueous phase using 50 ml dichloromethane three times. The aqueous phase was concentrated in vacuo and separated on a Phenomenex Synergi 4 µm Hydro-RP 80 Å column (250 × 10 mm) using an Agilent 1260 Infinity II HPLC system. Mobile phase A was water + 0.1% (v/v) formic acid and mobile phase B was acetonitrile + 0.1% (v/v) formic acid. The flow rate was kept at 3 ml min^{-1} and the gradient was as follows: 0% B (0–10 min), increase to 5% B (10–11 min), 5% B (11–21 min), increase to 100% B (21–22 min), 100% B (22–32 min), decrease to 0% B (32–33 min), 0% B (33–43 min). Apo-coelichelin eluted at 17.7–17.9 min and was collected by monitoring the absorbance at 210 nm. The collected apo-coelichelin was concentrated in vacuo, lyophilised and obtained as a white solid. The HR-ESI mass spectrometry data of apo-coelichelin was obtained on a Thermo Scientific Finnigan LTQ Orbitrap XL mass spectrometer equipped with a nano-electrospray ionization source operated in positive ionization mode. The data were analysed using Xcalibur 4.0 software. HR-ESI-MS (positive-ion mode): *m/z* 566.2776 $[M + H]^+$ (calculated for $C_{21}H_{40}N_7O_{11}^+$: 566.2780).

Coelichelin purity check by LC–MS

The purified coelichelin was analysed on a Phenomenex Synergi 4 µm Hydro-RP 80 Å column (250 × 4.6 mm) using an Agilent 1260 Infinity II HPLC system coupled to an Agilent InfinityLab LC/MSD XT mass spectrometer. Mobile phase A was water + 0.1% (v/v) formic acid and mobile phase B was acetonitrile + 0.1% (v/v) formic acid. The flow rate was kept at 0.7 ml min^{-1} and the gradient was as follows: 0% B (0–10 min), increase to 5% B (10–30 min), increase to 100% B (30–31 min), 100% B (31–41 min), decrease to 0% B (41–42 min), 0% B (42–52 min).

Preparation of Ga–coelichelin

Coelichelin (10 mg) was dissolved in 400 µl of water, followed by the addition of 26.5 mg of $Ga_2(SO_4)_3$ in 400 µl of water. The reaction was performed at room temperature for 30 min and subjected to separation on a Phenomenex Synergi 4 µm Hydro-RP 80 Å column (250 × 10 mm) using an Agilent 1260 Infinity II HPLC system. Mobile phase A was water + 0.1% (v/v) formic acid and mobile phase B was acetonitrile + 0.1% (v/v) formic acid. The flow rate was kept at 3 ml min^{-1} and the gradient was as follows: 0% B (0–10 min), increase to 100% B (10–11 min), 100% B (11–21 min), decrease to 0% B (21–22 min), 0% B (22–32 min). Ga–coelichelin eluted at 4.6–5.0 min and was collected by monitoring the absorbance at 210 nm. The collected Ga–coelichelin was concentrated in vacuo, lyophilised and obtained as a white solid. HR-ESI-MS (positive-ion mode): *m/z* 632.1794 $[M + H]^+$ (calculated for $C_{21}H_{37}GaN_7O_{11}^+$: 632.1801). ^1H and TOCSY (mixing time of 60 ms) NMR spectra were obtained on a Varian 600 MHz Inova NMR spectrometer using Varian/Agilent VnmrJ and Linux workstations. ^{13}C, DQF-COSY, HSQC and HMBC NMR spectra were obtained on a Bruker 500 MHz Avance Neo NMR spectrometer using Bruker IconNMR 5.1.9 software. All spectra were analysed using MestReNova 14.2.0-26256 software.

Iron complementation experiment

An overnight culture of *B. subtilis* RM125 WT was diluted 1:10 into 5 ml fresh ISP2 + 0.1 mM $MnCl_2$ + 5 mM $MgCl_2$, and poured onto an ISP2 + 0.1 mM $MnCl_2$ + 5 mM $MgCl_2$ + 1.5% agar plate. Bacteria were allowed 10 min to soak the plate and the unattached bacteria were then removed. The plate was dried under room temperature in a biosafety cabinet. A volume of 2 µl of compound was spotted as a small circle on top of the bacterial lawn. After the compound dried, 2 µl of $FeSO_4$ aqueous solution was spotted on top of the compound-treated area. After the $FeSO_4$ solution dried, the plate was incubated at 37 °C for 1 h. Then 5 µl of SPO1 phage lysate (~10 p.f.u.) was spotted on top of the compound-treated area. After the phage lysate dried, the plate was incubated at 37 °C and the size of plaques formed by SPO1 was quantified using Fiji[58] after 2 days.

Quantification of phage reproduction from individual plaques

An overnight culture of *B. subtilis* RM125 WT was diluted 1:10 into 5 ml fresh ISP2 + 0.1 mM $MnCl_2$ + 5 mM $MgCl_2$, and poured onto an ISP2 + 0.1 mM $MnCl_2$ + 5 mM $MgCl_2$ + 1.5% agar plate. Bacteria were allowed 10 min to attach to the plate and the unattached bacteria were then removed. The plate was dried under room temperature in a biosafety cabinet. EDDHA (2 µl, 6 mM) or water was spotted as a small circle on top of the bacterial lawn. After the compound dried, the plate was incubated at 37 °C for 1 h. Then 5 µl of SPO1 phage lysate (10–40 p.f.u.) was spotted on top of the compound-treated area. After the phage lysate dried, the plate was incubated at 37 °C for 2 days. The number of plaques formed in each phage spot was enumerated and the average plaque area for each phage spot was quantified using Fiji[58]. All the plaques in one phage spot were pooled by carving out the agar containing the plaques and resuspending in 5 ml phage buffer (10 mM Tris, 10 mM $MgSO_4$, 4 g l^{-1} NaCl, pH 7.5). The suspension was vortexed at the highest speed for 20 s to allow phages to fully detach from the agar. The p.f.u. of the pooled plaques were quantified using the small drop plaque assay[63]. For each individual phage spot, the average p.f.u. per plaque was calculated using the following equation:

$$\text{Avg.p.f.u. per plaque} = \frac{\text{p.f.u. of pooled plaques}}{\text{number of plaques}}$$

Sporulation quantification

B. subtilis spores were quantified by determining the number of colony-forming units (c.f.u.) after heat-treating the population to kill vegetative cells[64]. An overnight culture of *B. subtilis* RM125 WT was diluted 1:10 into 5 ml fresh ISP2 + 0.1 mM $MnCl_2$ + 5 mM $MgCl_2$, and poured onto an ISP2 + 0.1 mM $MnCl_2$ + 5 mM $MgCl_2$ + 1.5% agar plate. Bacteria were allowed 10 min to attach to the plate and the unattached bacteria were then removed. The plate was dried under room temperature in a biosafety cabinet. A volume of 2 µl of compound or water (control) was spotted as a small circle on top of the bacterial lawn. After the compound dried, the plate was incubated at 37 °C for 16 h. Then ~1 cm^2 area of bacteria was scraped off the plate and resuspended in 200 µl water. The cell suspension was heated at 85 °C for 15 min to kill non-sporulated cells. Then the spores in the heat-treated cell suspension were quantified by measuring the c.f.u.

Generation of sporulation mutants

The gene knockout donor in *B. subtilis* 168 were purchased from the Bacillus Genomic Stock Center. The mutation was then transferred to *B. subtilis* RM125 using SPP1-mediated generalized phage transduction[65,66]. Briefly, the SPP1 phage lysate was obtained from the *B. subtilis* 168 knockout donor strain as described above and stored at 4 °C until ready to use. A single colony of the recipient *B. subtilis* RM125 was inoculated into 10 ml LB + 10 mM $CaCl_2$. The recipient culture was incubated at 37 °C and 220 r.p.m. for 4 h. For phage transduction, 950 µl of the recipient culture was mixed with 50 µl of donor SPP1 lysate and incubated at 37 °C for 10 min to allow phage adsorption. Then the 1 ml infected culture was transferred into 9 ml of prewarmed LB + 20 mM sodium citrate and incubated at 37 °C for another 10 min. The cells were pelleted at 4,000 × *g* for 5 min and plated onto an LB + 20 mM sodium citrate + 1.5% agar plate with appropriate antibiotics. The plates were incubated at 37 °C overnight and the mutant colonies were restreaked twice on LB + 20 mM sodium citrate + 1.5% agar plate with appropriate

antibiotics to clean out phages. The knockout mutation was validated using PCR with primers reported in ref. 67. The sporulation mutants were verified to not produce spores using the sporulation quantification experiment described above.

Spo0A (sad67-D56N) restricts phage infection

An overnight culture of *B. subtilis* (BDR2345/BDR2349) was diluted 1:10 into 5 ml fresh ISP2 + 0.1 mM $MnCl_2$ + 5 mM $MgCl_2$ + 1 mM IPTG, and poured onto an ISP2 + 0.1 mM $MnCl_2$ + 5 mM $MgCl_2$ + 1 mM IPTG + 1.5% agar plate. Bacteria were allowed 10 min to attach to the plate and the unattached bacteria were then removed. The plate was dried under room temperature in a biosafety cabinet and then incubated at 37 °C for 1 h. After incubation, 5 µl of SPO1 phage lysate (~10 p.f.u.) was spotted on top of the compound-treated area. After the phage lysate dried, the plate was incubated at 37 °C and the size of plaques formed by SPO1 was quantified using Fiji[58] after 2 days.

Streptomyces sp. I8-5 and *B. subtilis* competition

To inoculate plates with *Streptomyces*, 5 µl of the frozen spore stock of I8-5 was suspended in 50 µl of ISP2 + 0.1 mM $MnCl_2$ + 5 mM $MgCl_2$. Then 8 µl of the spore suspension was spotted at the centre of an ISP2 + 0.1 mM $MnCl_2$ + 5 mM $MgCl_2$ + 1.5% agar plate. The plates were incubated at 30 °C for 16 days to allow the I8-5 colony to grow and secrete coelichelin into the plate. To inoculate the *B. subtilis* next to *Streptomyces*, an overnight culture of *B. subtilis* RM125 WT was diluted 1:10 into 5 ml fresh ISP2 + 0.1 mM $MnCl_2$ + 5 mM $MgCl_2$, and poured around the I8-5 colony. *B. subtilis* cells were allowed 10 min to attach to the plate and the unattached bacteria were then removed. The plate was dried under room temperature in a biosafety cabinet. Water (2 µl) or ferrioxamine E (20 mM solution in 2 µl water) was spotted as a small circle on top of the *B. subtilis* lawn. After the spotted solution dried, the plate was incubated at 37 °C for 1 h. Then 5 µl of SPO1 phage lysate (~10 p.f.u.) was spotted on top of the compound-treated area. After the phage lysate dried, the plate was incubated at 37 °C for 2 days. The average plaque area for each phage spot was quantified using Fiji[58]. The *B. subtilis* lawn and *Streptomyces* colony were carved out and resuspended in 5 ml LB broth and 5 ml ISP2 medium, respectively. The cell suspensions were vortexed at the highest speed for 20 s to allow bacterial cells to fully detach from the agar. The c.f.u. of *B. subtilis* cell suspensions were quantified by plating serial dilutions of the cell suspension on LB + 1.5% agar plates. The c.f.u. of *Streptomyces* cell suspensions were quantified by plating serial dilutions of the cell suspension on ISP2 + 10 µg ml^{-1} nalidixic acid + 1.5% agar plates.

Test of phage promotion activity of Actinomycetia

To prepare plates with Actinomycetia, 5 µl of the frozen spore stock of each bacterial strain in our library was suspended in 50 µl of ISP2 medium. Then 8 µl of the spore suspension was spotted at the centre of an ISP2 + 0.1 mM $MnCl_2$ + 5 mM $MgCl_2$ + 1.5% agar plate. The inoculated plates were incubated at 30 °C for 10 days to allow Actinomycetia to grow and secrete their metabolites into the plate. To test the influence of the metabolites on phage infectivity, an overnight culture of *B. subtilis* RM125 WT was diluted 1:10 into 5 ml fresh ISP2 + 0.1 mM $MnCl_2$ + 5 mM $MgCl_2$, and poured around the Actinomycetia colony. *B. subtilis* were allowed 10 min to attach to the plate and the unattached bacteria were then removed. The plate was dried under room temperature in a biosafety cabinet and then incubated at 37 °C for 1 h. After incubation, 5 µl of SPO1 phage lysate (~10 p.f.u.) was spotted on top of the *B. subtilis* lawn. After the phage lysate dried, the plate was incubated at 37 °C and the size of plaques formed by SPO1 was quantified using Fiji[58] after 2 days.

Detection of coelichelin production by Actinomycetia

To revive the spores of Actinomycetia, 5 µl of the Actinomycetia frozen spore stock was streaked out on an ISP2 + 1.5% agar plate. The plate was incubated at 30 °C for 3 days until colonies formed. A colony was inoculated into 4 ml fresh ISP2 medium and incubated at 30 °C and 220 r.p.m. for 4 days. After the incubation, 1 ml of the culture was added into 100 ml of ISP2 medium + 0.1 mM $MnCl_2$ + 5 mM $MgCl_2$ and incubated at 30 °C and 220 r.p.m. To monitor the coelichelin level in the growth media, 1 ml of culture was removed and centrifuged at 16,000 × *g* for 5 min. Then the supernatant was collected and filtered through a 0.2 µm polyethersulfone filter. Of the supernatant, 10 µl was analysed on a Phenomenex Synergi 4 µm Hydro-RP 80 Å column (250 × 4.6 mm) using an Agilent 1260 Infinity II HPLC system coupled to an Agilent InfinityLab LC/MSD XT mass spectrometer. Mobile phase A was water + 0.1% (v/v) formic acid and mobile phase B was acetonitrile + 0.1% (v/v) formic acid. The flow rate was kept at 0.7 ml min^{-1} and the gradient was as follows: 0% B (0–20 min), increase to 20% B (20–21 min), increase to 40% B (21–31 min), increase to 100% B (31–32 min), 100% B (32–42 min), decrease to 0% B (42–43 min), 0% B (43–48 min).

Reporting summary

Further information on research design is available in the Nature Portfolio Reporting Summary linked to this article.

Data availability

The genome sequence of strain I8-5 is available on NCBI (accession number JAYMFC000000000). The 16S sequences of the other plaque-enlarging bacteria are available on NCBI (I8-5: GenBank OR902106; Am9: GenBank PQ178887; Am23: GenBank PQ178944; Am62: GenBank PQ178965; R1B3: GenBank PQ178995; I8-24: GenBank PQ179041). Source data for plaque measurements are available on figshare at https://doi.org/10.6084/m9.figshare.27269481 (ref. 68). Any further requests for data should be addressed to the corresponding author (jpgerdt@iu.edu).

References

1. Hibbing, M. E., Fuqua, C., Parsek, M. R. & Peterson, S. B. Bacterial competition: surviving and thriving in the microbial jungle. *Nat. Rev. Microbiol.* **8**, 15–25 (2010).
2. Ghoul, M. & Mitri, S. The ecology and evolution of microbial competition. *Trends Microbiol.* **24**, 833–845 (2016).
3. Westhoff, S., Kloosterman, A. M., Hoesel, S. F. A. V., Wezel, G. P. V. & Rozen, D. E. Competition sensing changes antibiotic production in *Streptomyces*. *mBio* **12**, e02729-20 (2021).
4. Valle, J. et al. Broad-spectrum biofilm inhibition by a secreted bacterial polysaccharide. *Proc. Natl Acad. Sci. USA* **103**, 12558–12563 (2006).
5. Kramer, J., Özkaya, Ö. & Kümmerli, R. Bacterial siderophores in community and host interactions. *Nat. Rev. Microbiol.* **18**, 152–163 (2020).
6. Suttle, C. A. The significance of viruses to mortality in aquatic microbial communities. *Microb. Ecol.* **28**, 237–243 (1994).
7. Koskella, B. & Meaden, S. Understanding bacteriophage specificity in natural microbial communities. *Viruses* **5**, 806–823 (2013).
8. Hampton, H. G., Watson, B. N. J. & Fineran, P. C. The arms race between bacteria and their phage foes. *Nature* **577**, 327–336 (2020).
9. Otsuji, N., Sekiguchi, M., Iijima, T. & Takagi, Y. Induction of phage formation in the lysogenic *Escherichia coli* K-12 by mitomycin C. *Nature* **184**, 1079–1080 (1959).
10. Jancheva, M. & Böttcher, T. A metabolite of *Pseudomonas* triggers prophage-selective lysogenic to lytic conversion in *Staphylococcus aureus*. *J. Am. Chem. Soc.* **143**, 8344–8351 (2021).
11. Silpe, J. E., Wong, J. W. H., Owen, S. V., Baym, M. & Balskus, E. P. The bacterial toxin colibactin triggers prophage induction. *Nature* **603**, 315–320 (2022).

12. Hardy, A., Kever, L. & Frunzke, J. Antiphage small molecules produced by bacteria – beyond protein-mediated defenses. *Trends Microbiol.* **31**, 92–106 (2023).
13. Lautru, S., Deeth, R. J., Bailey, L. M. & Challis, G. L. Discovery of a new peptide natural product by *Streptomyces coelicolor* genome mining. *Nat. Chem. Biol.* **1**, 265–269 (2005).
14. Williams, J. C. et al. Synthesis of the siderophore coelichelin and its utility as a probe in the study of bacterial metal sensing and response. *Org. Lett.* **21**, 679–682 (2019).
15. Challis, G. L. & Ravel, J. Coelichelin, a new peptide siderophore encoded by the *Streptomyces coelicolor* genome: structure prediction from the sequence of its non-ribosomal peptide synthetase. *FEMS Microbiol. Lett.* **187**, 111–114 (2000).
16. Hider, R. C. & Kong, X. Chemistry and biology of siderophores. *Nat. Prod. Rep.* **27**, 637–657 (2010).
17. May, J. J., Wendrich, T. M. & Marahiel, M. A. The dhb operon of *Bacillus subtilis* encodes the biosynthetic template for the catecholic siderophore 2,3-dihydroxybenzoate-glycine-threonine trimeric ester bacillibactin. *J. Biol. Chem.* **276**, 7209–7217 (2001).
18. Schneider, R. & Hantke, K. Iron-hydroxamate uptake systems in *Bacillus subtilis*: identification of a lipoprotein as part of a binding protein-dependent transport system. *Mol. Microbiol.* **8**, 111–121 (1993).
19. Abergel, R. J., Zawadzka, A. M., Hoette, T. M. & Raymond, K. N. Enzymatic hydrolysis of trilactone siderophores: where chiral recognition occurs in enterobactin and bacillibactin iron transport. *J. Am. Chem. Soc.* **131**, 12682–12692 (2009).
20. Dertz, E. A., Xu, J., Stintzi, A. & Raymond, K. N. Bacillibactin-mediated iron transport in *Bacillus subtilis*. *J. Am. Chem. Soc.* **128**, 22–23 (2006).
21. Ollinger, J., Song, K.-B., Antelmann, H., Hecker, M. & Helmann, J. D. Role of the fur regulon in iron transport in *Bacillus subtilis*. *J. Bacteriol.* **188**, 3664–3673 (2006).
22. Gallet, R., Kannoly, S. & Wang, I.-N. Effects of bacteriophage traits on plaque formation. *BMC Microbiol.* **11**, 181 (2011).
23. Zang, Z., Park, K. J. & Gerdt, J. P. A metabolite produced by gut microbes represses phage infections in *Vibrio cholerae*. *ACS Chem. Biol.* **17**, 2396–2403 (2022).
24. Bokinsky, G. et al. HipA-triggered growth arrest and beta-lactam tolerance in *Escherichia coli* are mediated by RelA-dependent ppGpp synthesis. *J. Bacteriol.* **195**, 3173–3182 (2013).
25. Woody, M. A. & Cliver, D. O. Effects of temperature and host cell growth phase on replication of F-specific RNA coliphage Q beta. *Appl. Environ. Microbiol.* **61**, 1520–1526 (1995).
26. Bryan, D., El-Shibiny, A., Hobbs, Z., Porter, J. & Kutter, E. M. Bacteriophage T4 infection of stationary phase *E. coli*: life after log from a phage perspective. *Front. Microbiol.* **7**, 1391 (2016).
27. Los, M. et al. Effective inhibition of lytic development of bacteriophages lambda, P1 and T4 by starvation of their host, *Escherichia coli*. *BMC Biotechnol.* **7**, 13 (2007).
28. Rittershaus, E. S. C., Baek, S.-H. & Sassetti, C. M. The normalcy of dormancy: common themes in microbial quiescence. *Cell Host Microbe* **13**, 643–651 (2013).
29. Phillips, Z. E. & Strauch, M. A. *Bacillus subtilis* sporulation and stationary phase gene expression. *Cell. Mol. Life Sci.* **59**, 392–402 (2002).
30. Ireton, K., Rudner, D. Z., Siranosian, K. J. & Grossman, A. D. Integration of multiple developmental signals in *Bacillus subtilis* through the Spo0A transcription factor. *Genes Dev.* **7**, 283–294 (1993).
31. Grandchamp, G. M., Caro, L. & Shank, E. A. Pirated siderophores promote sporulation in *Bacillus subtilis*. *Appl. Environ. Microbiol.* **83**, e03293–03216 (2017).
32. Qin, Y. et al. Heterogeneity in respiratory electron transfer and adaptive iron utilization in a bacterial biofilm. *Nat. Commun.* **10**, 3702 (2019).
33. Molle, V. et al. The Spo0A regulon of *Bacillus subtilis*. *Mol. Microbiol.* **50**, 1683–1701 (2003).
34. Zhu, M. et al. A fitness trade-off between growth and survival governed by Spo0A-mediated proteome allocation constraints in *Bacillus subtilis*. *Sci. Adv.* **9**, eadg9733 (2023).
35. Hoch, J. A. Regulation of the phosphorelay and the initiation of sporulation in *Bacillus subtilis*. *Annu. Rev. Microbiol.* **47**, 441–465 (1993).
36. Măgălie, A. et al. Phage infection fronts trigger early sporulation and collective defense in bacterial populations. Preprint at *bioRxiv* https://doi.org/10.1101/2024.05.22.595388 (2024).
37. Schwartz, D. A., Lehmkuhl, B. K. & Lennon, J. T. Phage-encoded sigma factors alter bacterial dormancy. *mSphere* **7**, e00297-22 (2022).
38. Tan, I. S. & Ramamurthi, K. S. Spore formation in *Bacillus subtilis*. *Environ. Microbiol. Rep.* **6**, 212–225 (2014).
39. Pires, D. P., Melo, L. D. R. & Azeredo, J. Understanding the complex phage–host interactions in biofilm communities. *Annu. Rev. Virol.* **8**, 73–94 (2021).
40. Banse, A. V., Chastanet, A., Rahn-Lee, L., Hobbs, E. C. & Losick, R. Parallel pathways of repression and antirepression governing the transition to stationary phase in *Bacillus subtilis*. *Proc. Natl Acad. Sci. USA* **105**, 15547–15552 (2008).
41. McLoon, A. L., Guttenplan, S. B., Kearns, D. B., Kolter, R. & Losick, R. Tracing the domestication of a biofilm-forming bacterium. *J. Bacteriol.* **193**, 2027–2034 (2011).
42. van Sinderen, D. et al. comK encodes the competence transcription factor, the key regulatory protein for competence development in *Bacillus subtilis*. *Mol. Microbiol.* **15**, 455–462 (1995).
43. González-Pastor, J. E., Hobbs, E. C. & Losick, R. Cannibalism by sporulating bacteria. *Science* **301**, 510–513 (2003).
44. Ellermeier, C. D., Hobbs, E. C., Gonzalez-Pastor, J. E. & Losick, R. A three-protein signaling pathway governing immunity to a bacterial cannibalism toxin. *Cell* **124**, 549–559 (2006).
45. Straight, P. D., Willey, J. M. & Kolter, R. Interactions between *Streptomyces coelicolor* and *Bacillus subtilis*: role of surfactants in raising aerial structures. *J. Bacteriol.* **188**, 4918–4925 (2006).
46. Hemphill, H. E. & Whiteley, H. R. Bacteriophages of *Bacillus subtilis*. *Bacteriol. Rev.* **39**, 257–315 (1975).
47. Willms, I. M., Hoppert, M. & Hertel, R. Characterization of *Bacillus subtilis* viruses vB_BsuM-Goe2 and vB_BsuM-Goe3. *Viruses* **9**, 146 (2017).
48. Liu, C. G. et al. Phage–antibiotic synergy is driven by a unique combination of antibacterial mechanism of action and stoichiometry. *mBio* **11**, e01462-20 (2020).
49. Niehus, R., Picot, A., Oliveira, N. M., Mitri, S. & Foster, K. R. The evolution of siderophore production as a competitive trait. *Evolution* **71**, 1443–1455 (2017).
50. Henriques, A. O. & Moran, C. P. Jr Structure, assembly, and function of the spore surface layers. *Annu. Rev. Microbiol.* **61**, 555–588 (2007).
51. Nicholson, W. L., Munakata, N., Horneck, G., Melosh, H. J. & Setlow, P. Resistance of *Bacillus* endospores to extreme terrestrial and extraterrestrial environments. *Microbiol. Mol. Biol. Rev.* **64**, 548–572 (2000).
52. Lennon, J. T. & Jones, S. E. Microbial seed banks: the ecological and evolutionary implications of dormancy. *Nat. Rev. Microbiol.* **9**, 119–130 (2011).
53. Khanna, K., Lopez-Garrido, J. & Pogliano, K. Shaping an endospore: architectural transformations during *Bacillus subtilis* sporulation. *Annu. Rev. Microbiol.* **74**, 361–386 (2020).
54. Schwartz, D. A. et al. Human-gut phages harbor sporulation genes. *mBio* **14**, e0018223 (2023).

55. Xiong, Q. et al. Autoinducer-2 relieves soil stress-induced dormancy of *Bacillus velezensis* by modulating sporulation signaling. *npj Biofilms Microbiomes* **10**, 117 (2024).
56. Aldape, M. J. et al. Fidaxomicin reduces early toxin A and B production and sporulation in *Clostridium difficile* in vitro. *J. Med. Microbiol.* **66**, 1393–1399 (2017).
57. Golonka, R., Yeoh, Beng, S. & Vijay-Kumar, M. The iron tug-of-war between bacterial siderophores and innate immunity. *J. Innate Immun.* **11**, 249–262 (2019).
58. Schindelin, J. et al. Fiji: an open-source platform for biological-image analysis. *Nat. Methods* **9**, 676–682 (2012).
59. Bolger, A. M., Lohse, M. & Usadel, B. Trimmomatic: a flexible trimmer for Illumina sequence data. *Bioinformatics* **30**, 2114–2120 (2014).
60. Prjibelski, A., Antipov, D., Meleshko, D., Lapidus, A. & Korobeynikov, A. Using SPAdes De Novo Assembler. *Curr. Protoc. Bioinform.* **70**, e102 (2020).
61. Seemann, T. Prokka: rapid prokaryotic genome annotation. *Bioinformatics* **30**, 2068–2069 (2014).
62. Blin, K. et al. AntiSMASH 7.0: new and improved predictions for detection, regulation, chemical structures and visualisation. *Nucleic Acids Res.* **51**, W46–W50 (2023).
63. Mazzocco, A., Waddell, T. E., Lingohr, E. & Johnson, R. P. in *Bacteriophages: Methods and Protocols Volume 1: Isolation, Characterization, and Interactions* (eds Clokie, M. & Kropinski, A.) 81–85 (Humana Press, 2009).
64. Siala, A., Hill, I. R. & Gray, T. R. G. Populations of spore-forming bacteria in an acid forest soil, with special reference to *Bacillus subtilis*. *Microbiology* **81**, 183–190 (1974).
65. Yasbin, R. E. & Young, F. E. Transduction in *Bacillus subtilis* by bacteriophage SPP1. *J. Virol.* **14**, 1343–1348 (1974).
66. Konkol, M. A., Blair, K. M. & Kearns, D. B. Plasmid-encoded ComI inhibits competence in the ancestral 3610 strain of *Bacillus subtilis*. *J. Bacteriol.* **195**, 4085–4093 (2013).
67. Koo, B.-M. et al. Construction and analysis of two genome-scale deletion libraries for *Bacillus subtilis*. *Cell Syst.* **4**, 291–305.e297 (2017).
68. Zang, Z. et al. *Streptomyces* secretes a siderophore that sensitizes competitor bacteria to phage infection. *figshare* https://doi.org/10.6084/m9.figshare.27269481 (2024).

Acknowledgements

We thank A. Măgălie (Georgia Institute of Technology) and J. Weitz (University of Maryland) for helpful discussions; the Bacillus Genomic Stock Center (Ohio State University), the Félix d'Hérelle Reference Center for Bacterial Viruses (University of Laval), R. Hertel (University of Goettingen) and D. Rudner (Harvard Medical School) for providing bacteria and phages; and E. M. Nolan (Massachusetts Institute of Technology) for providing enterobactin. The research was supported by a research starter grant from the American Society of Pharmacognosy to J.P.G. and a National Science Foundation CAREER award (IOS-2143636) to J.P.G. Research support was also provided by the National Science Foundation (DEB-1934554 to J.T.L. and D.A.S.; DBI-2022049 to J.T.L.), the US Army Research Office (W911NF-22-1-0014 and W911NF-22-S-0008 to J.T.L.) and the National Aeronautics and Space Administration (80NSSC20K0618 to J.T.L.). Z.Z. was supported in part by the John R. and Wendy L. Kindig Fellowship. K.J.P. and the Laboratory for Biological Mass Spectrometry were supported by the Indiana University Precision Health Initiative. The 500 MHz NMR and 600 MHz spectrometer of the Indiana University NMR facility were supported by NSF grant CHE-1920026, and the Prodigy probe was purchased in part with support from the Indiana Clinical and Translational Sciences Institute, funded in part by NIH Award TL1TR002531.

Author contributions

Z.Z. and J.P.G. conceptualized the project. Z.Z., D.A.S. and J.P.G. developed the methodology. Z.Z., C.Z., K.J.P. and R.P. conducted investigations. Z.Z. and J.P.G. wrote the original draft of the paper. Z.Z., C.Z., D.A.S., J.T.L. and J.P.G. reviewed and edited the paper. Z.Z. and J.P.G. performed visualization. J.T.L. and J.P.G. supervised the project. J.T.L. and J.P.G. acquired funding.

Competing interests

The authors declare no competing interests.

Additional information

Extended data is available for this paper at https://doi.org/10.1038/s41564-024-01910-8.

Supplementary information The online version contains supplementary material available at https://doi.org/10.1038/s41564-024-01910-8.

Correspondence and requests for materials should be addressed to Joseph P. Gerdt.

Peer review information *Nature Microbiology* thanks Anna Dragos, Justin Nodwell and the other, anonymous, reviewer(s) for their contribution to the peer review of this work. Peer reviewer reports are available.

https://doi.org/10.1038/s41564-024-01910-8

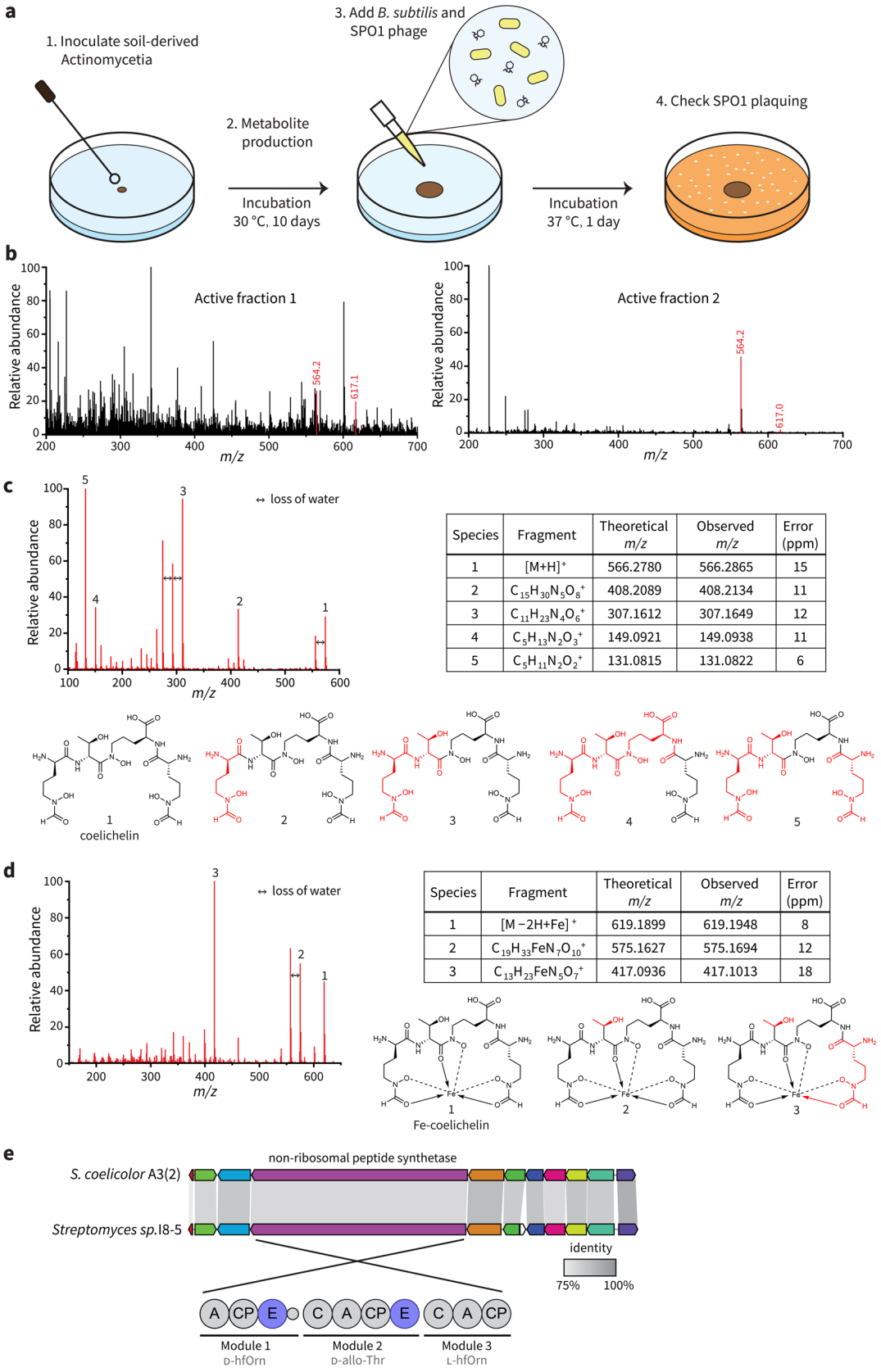

Species	Fragment	Theoretical *m/z*	Observed *m/z*	Error (ppm)
1	$[M+H]^+$	566.2780	566.2865	15
2	$C_{15}H_{30}N_5O_8^+$	408.2089	408.2134	11
3	$C_{11}H_{23}N_4O_6^+$	307.1612	307.1649	12
4	$C_5H_{13}N_2O_3^+$	149.0921	149.0938	11
5	$C_5H_{11}N_2O_2^+$	131.0815	131.0822	6

Species	Fragment	Theoretical *m/z*	Observed *m/z*	Error (ppm)
1	$[M-2H+Fe]^+$	619.1899	619.1948	8
2	$C_{19}H_{33}FeN_7O_{10}^+$	575.1627	575.1694	12
3	$C_{13}H_{23}FeN_5O_7^+$	417.0936	417.1013	18

Extended Data Fig. 1 | See next page for caption.

https://doi.org/10.1038/s41564-024-01910-8

Extended Data Fig. 1 | Coelichelin is the active metabolite that promotes phage predation. (**a**) Scheme of the binary-interaction screen. (**b**) Negative mode electrospray ionization MS spectra of active fraction 1 (left) and active fraction 2 (right). The shared peaks are highlighted red. (**c**) MS/MS spectrum of the *m/z* 566.2783 species. Key fragments are annotated with their associated peak, and their losses are highlighted in red. (**d**) MS/MS spectrum of the *m/z* 619.1885 species. Key fragments are annotated with their associated peak, and their losses are highlighted in red. (**e**) Comparison of the *Streptomyces* sp. I8-5 coelichelin biosynthetic gene cluster with the reported one from *S. coelicolor* A3(2). The percent identity between each pair of genes is shown with shading (all were >75%). The modules of the coelichelin non-ribosomal peptide synthetase are shown in the lower region of the panel. The three modules are responsible for installation of D-δ-*N*-formyl-δ-*N*-hydroxyornithine (D-hfOrn), D-allo-threonine (D-allo-Thr), and L-δ-*N*-hydroxyornithine (L-hOrn), respectively. The adenylation domains (A), thiolation and peptide carrier proteins (CP), condensation domains (C), and epimerization domains (E) are shown.

https://doi.org/10.1038/s41564-024-01910-8

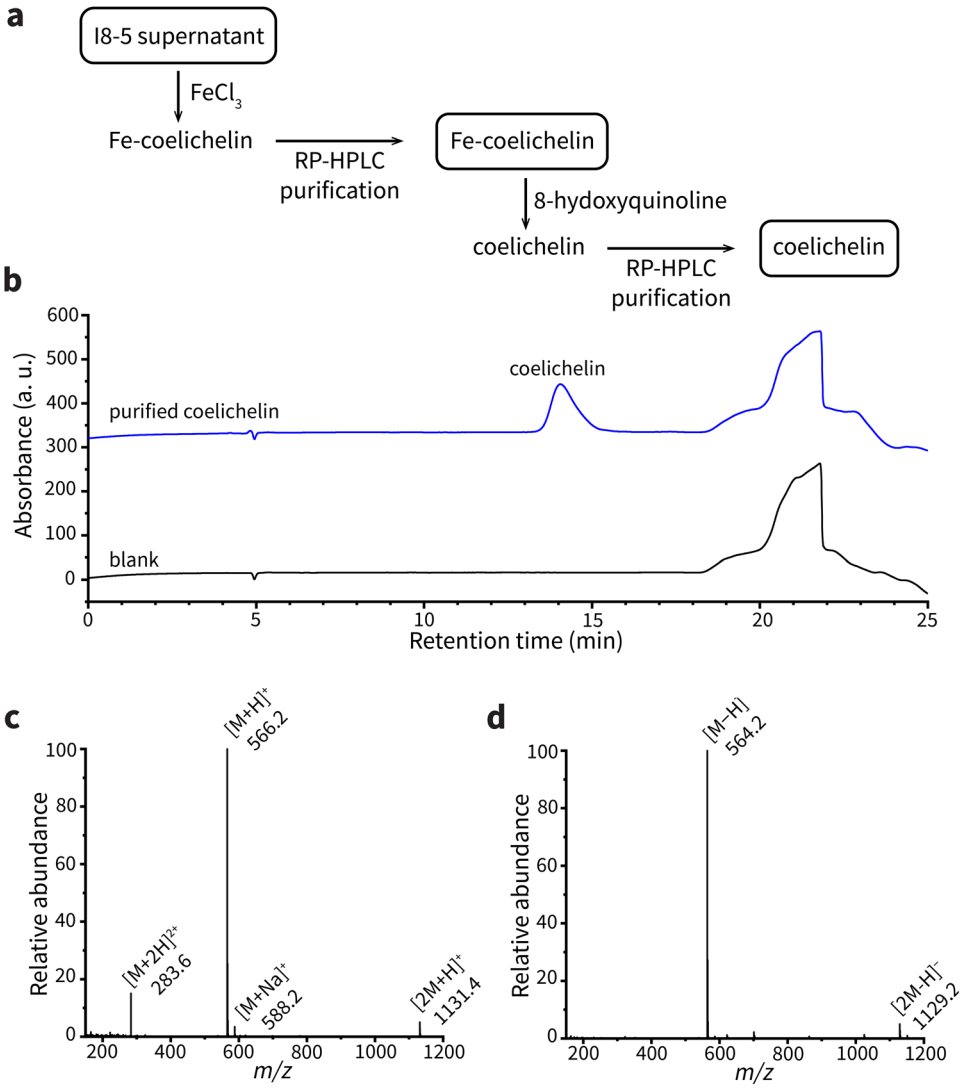

Extended Data Fig. 2 | Coelichelin isolation from I8-5 supernatant. (**a**) Isolation scheme. (**b**) UV chromatogram at 210 nm. Water was used as the blank. (**c**) The averaged MS spectrum at positive mode between retention time 13.5 ~ 14.8 min. (**d**) The averaged MS spectrum at negative mode between retention time 13.5 ~ 14.8 min. M represents coelichelin.

https://doi.org/10.1038/s41564-024-01910-8

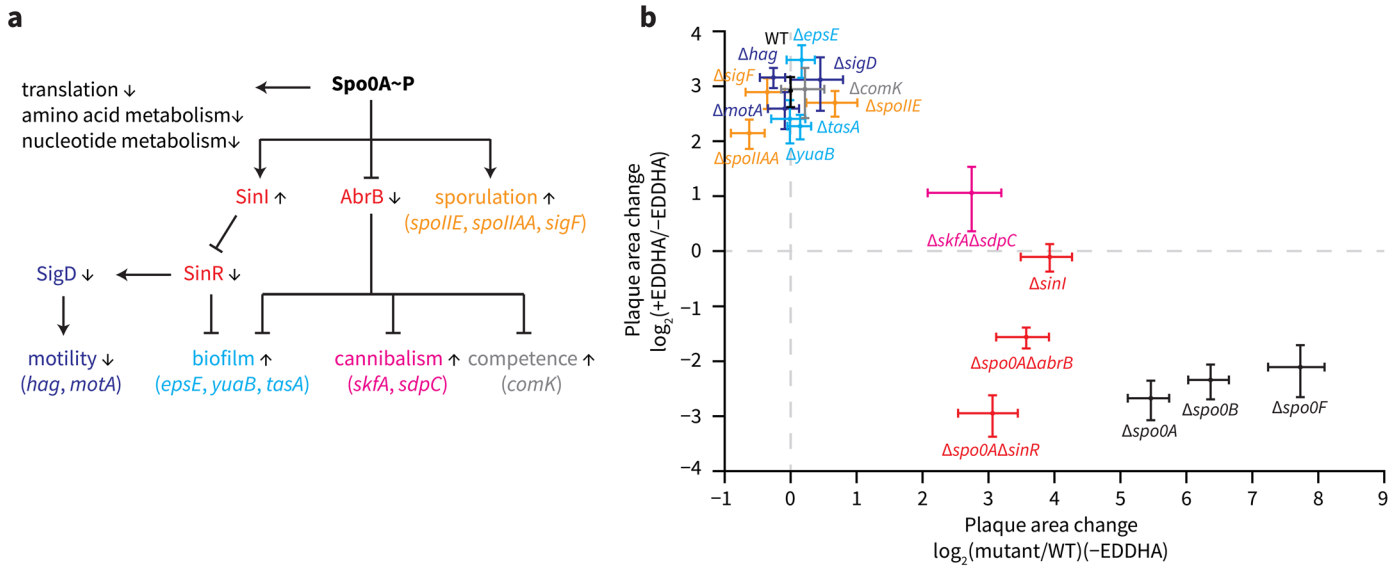

Extended Data Fig. 3 | Multiple pathways regulated by Spo0A are important for the plaque enlargement phenotype caused by iron sequestration. (**a**) Pathways regulated by Spo0A. (**b**) The x-axis shows the plaque size ratio between mutant and wild type (WT) under iron-rich conditions (− EDDHA). The y-axis shows the plaque size ratio between iron-limited (6 mM EDDHA treated [2 µL]) and iron-rich conditions (− EDDHA) of different mutants. Water was used as the −EDDHA control. Data are represented as the average ratio ± SEM calculated from at least four individual plaques of each condition.

https://doi.org/10.1038/s41564-024-01910-8

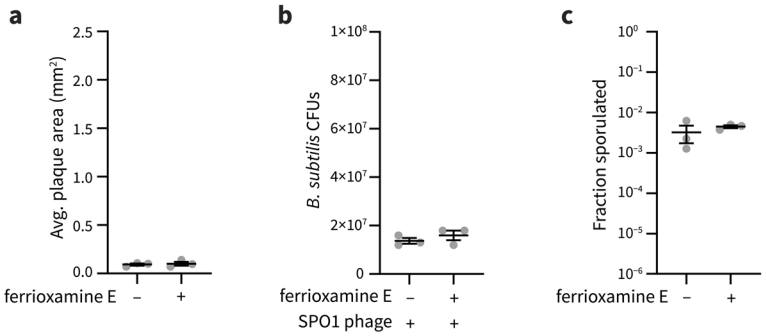

Extended Data Fig. 4 | Ferrioxamine E alone has no substantial effect on plaque size, *B. subtilis* growth, and Spo0A activation. (**a**) The average plaque areas of SPO1 on *B. subtilis* were measured when treated with or without ferrioxamine E (2 µl of 20 mM) as an excess iron source. Data are represented as the average ± SEM from three independent biological replicates. Circles show the values of each biological replicate and at least 21 plaques were selected for each replicate. (**b**) The colony forming units of *B. subtilis* were measured when infected by SPO1 phages, treated with or without ferrioxamine E (2 µl of 20 mM) as an excess iron source. Data are represented as the average ± SEM from three independent biological replicates. Circles show the values of each biological replicate. (**c**) The impact of ferrioxamine E (2 µl of 20 mM) on *B. subtilis* sporulation (an indicator of Spo0A activation). Data are represented as the average ± SEM from three independent biological replicates. Circles show the values of each biological replicate.

https://doi.org/10.1038/s41564-024-01910-8

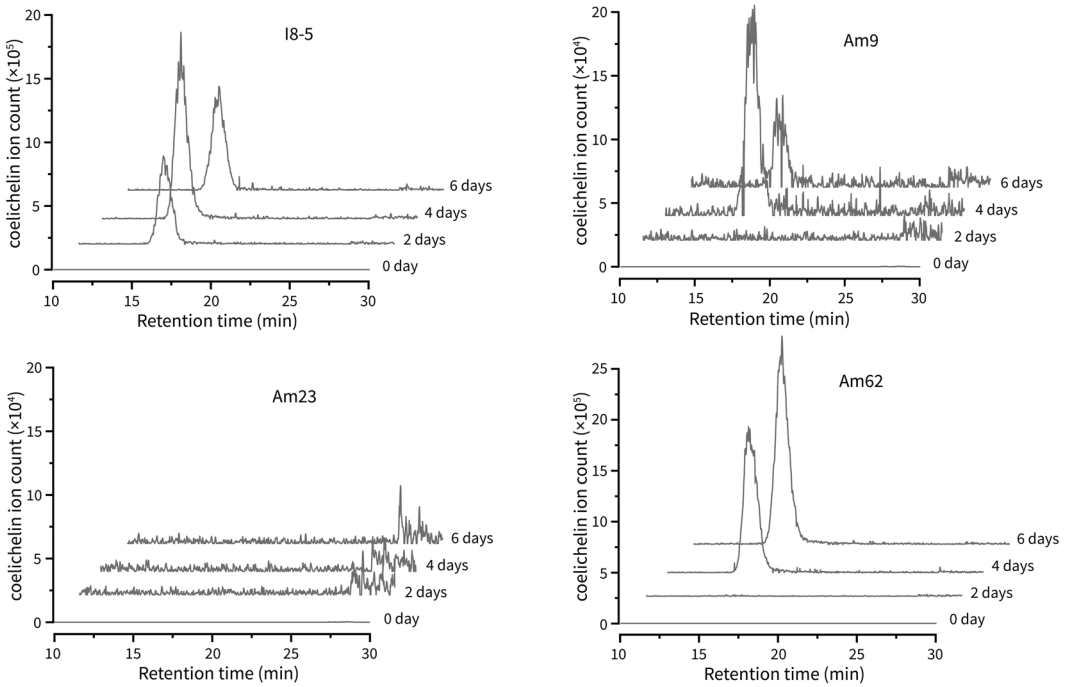

Extended Data Fig. 5 | Coelichelin is not ubiquitously produced by all plaque-enlarging bacteria. The conditioned media resulting from the fermentation of 4 plaque-enlarging bacteria (collected at different time points) were subjected to LC-MS analysis. The extracted ion chromatogram of coelichelin is shown here. No coelichelin was detected in the conditioned medium of Am23, suggesting that it does not produce coelichelin but instead an unknown phage-promoting siderophore.

nature portfolio

Corresponding author(s): Joseph P. Gerdt

Last updated by author(s): Nov 26, 2024

Reporting Summary

Nature Portfolio wishes to improve the reproducibility of the work that we publish. This form provides structure for consistency and transparency in reporting. For further information on Nature Portfolio policies, see our Editorial Policies and the Editorial Policy Checklist.

Statistics

For all statistical analyses, confirm that the following items are present in the figure legend, table legend, main text, or Methods section.

n/a	Confirmed	
☐	☒	The exact sample size (*n*) for each experimental group/condition, given as a discrete number and unit of measurement
☐	☒	A statement on whether measurements were taken from distinct samples or whether the same sample was measured repeatedly
☒	☐	The statistical test(s) used AND whether they are one- or two-sided *Only common tests should be described solely by name; describe more complex techniques in the Methods section.*
☒	☐	A description of all covariates tested
☒	☐	A description of any assumptions or corrections, such as tests of normality and adjustment for multiple comparisons
☐	☒	A full description of the statistical parameters including central tendency (e.g. means) or other basic estimates (e.g. regression coefficient) AND variation (e.g. standard deviation) or associated estimates of uncertainty (e.g. confidence intervals)
☒	☐	For null hypothesis testing, the test statistic (e.g. *F*, *t*, *r*) with confidence intervals, effect sizes, degrees of freedom and *P* value noted *Give P values as exact values whenever suitable.*
☒	☐	For Bayesian analysis, information on the choice of priors and Markov chain Monte Carlo settings
☒	☐	For hierarchical and complex designs, identification of the appropriate level for tests and full reporting of outcomes
☒	☐	Estimates of effect sizes (e.g. Cohen's *d*, Pearson's *r*), indicating how they were calculated

Our web collection on statistics for biologists contains articles on many of the points above.

Software and code

Policy information about availability of computer code

Data collection	NMR data were collected with vArian/Agilent VnmrJ 3.2 software, and Bruker IconNMR 5.9.1 software. LCMS data were collected with Agilent Openlab CDS Chemstation C.01.10 (low resolution) or Acquity UPLC 1.51.3347 and MassLynx 4.1 (high resolution)
Data analysis	FIJI (ImageJ2) 2.9.0/1.53t was used to measure plaque sizes, GraphPad Prism 10 was used to plot results, MestreNova 14.2.0 was used to analyze NMR data. LCMS data was analyzed with Agilent Openlab CDS ChemStation C.01.10 (low resolution) and MassLynx 4.1 (high resolution).

For manuscripts utilizing custom algorithms or software that are central to the research but not yet described in published literature, software must be made available to editors and reviewers. We strongly encourage code deposition in a community repository (e.g. GitHub). See the Nature Portfolio guidelines for submitting code & software for further information.

Data

Policy information about availability of data

All manuscripts must include a data availability statement. This statement should provide the following information, where applicable:

- Accession codes, unique identifiers, or web links for publicly available datasets
- A description of any restrictions on data availability
- For clinical datasets or third party data, please ensure that the statement adheres to our policy

Genome sequencing data are available from NCBI (accession number: JAYMFC000000000). 16S sequence data are available from NCBI (I8-5: GenBank OR902106;

Am9: GenBank PQ178887; Am23: GenBank PQ178944; Am62: GenBank PQ178965; R1B3: GenBank PQ178995; I8-24: GenBank PQ179041). Raw image, NMR, and LCMS data are available on Figshare (doi: 10.6084/m9.figshare.27269481).

Research involving human participants, their data, or biological material

Policy information about studies with human participants or human data. See also policy information about sex, gender (identity/presentation), and sexual orientation and race, ethnicity and racism.

Reporting on sex and gender	N/A
Reporting on race, ethnicity, or other socially relevant groupings	N/A
Population characteristics	N/A
Recruitment	N/A
Ethics oversight	N/A

Note that full information on the approval of the study protocol must also be provided in the manuscript.

Field-specific reporting

Please select the one below that is the best fit for your research. If you are not sure, read the appropriate sections before making your selection.

☒ Life sciences ☐ Behavioural & social sciences ☐ Ecological, evolutionary & environmental sciences

For a reference copy of the document with all sections, see nature.com/documents/nr-reporting-summary-flat.pdf

Life sciences study design

All studies must disclose on these points even when the disclosure is negative.

Sample size	Sample sizes were chosen based on experimental feasibility. At a minimum, triplicates were employed.
Data exclusions	no data were excluded.
Replication	None of the results reported could not be replicated. To ensure reproducibility, experiments were replicated the number of times reported in the figure captions and methods sections. Generally, the experiments were repeated at least once (with similar results), and the reported data in the manuscript are from a single-day experiment (with the reported number of replicate samples).
Randomization	Samples were not randomized, but all data to be compared were collected in parallel on the same data to eliminate any day-to-day variance.
Blinding	Experiments were not blinded. All measurements were quantitative and lacked subjective interpretation. Raw image data are retained for independent validation if needed.

Reporting for specific materials, systems and methods

We require information from authors about some types of materials, experimental systems and methods used in many studies. Here, indicate whether each material, system or method listed is relevant to your study. If you are not sure if a list item applies to your research, read the appropriate section before selecting a response.

Materials & experimental systems

n/a	Involved in the study
☒	☐ Antibodies
☒	☐ Eukaryotic cell lines
☒	☐ Palaeontology and archaeology
☒	☐ Animals and other organisms
☒	☐ Clinical data
☒	☐ Dual use research of concern
☒	☐ Plants

Methods

n/a	Involved in the study
☒	☐ ChIP-seq
☒	☐ Flow cytometry
☒	☐ MRI-based neuroimaging

Plants

Seed stocks

Report on the source of all seed stocks or other plant material used. If applicable, state the seed stock centre and catalogue number. If plant specimens were collected from the field, describe the collection location, date and sampling procedures.

Novel plant genotypes

Describe the methods by which all novel plant genotypes were produced. This includes those generated by transgenic approaches, gene editing, chemical/radiation-based mutagenesis and hybridization. For transgenic lines, describe the transformation method, the number of independent lines analyzed and the generation upon which experiments were performed. For gene-edited lines, describe the editor used, the endogenous sequence targeted for editing, the targeting guide RNA sequence (if applicable) and how the editor was applied.

Authentication

Describe any authentication procedures for each seed stock used or novel genotype generated. Describe any experiments used to assess the effect of a mutation and, where applicable, how potential secondary effects (e.g. second site T-DNA insertions, mosiacism, off-target gene editing) were examined.